

Proximity effects and characteristic lengths in ferromagnet-superconductor structures

Klaus Halterman[†] and Oriol T. Valls^{*}

School of Physics and Astronomy and Minnesota Supercomputer Institute, University of Minnesota, Minneapolis, Minnesota 55455-0149

(November 9, 2018)

We present an extensive theoretical investigation of the proximity effects that occur in Ferromagnet/Superconductor (F/S) systems. We use a numerical method to solve self consistently the Bogoliubov-de Gennes equations in the continuum. We obtain the pair amplitude and the local density of states (DOS), and use these results to extract the relevant lengths characterizing the leakage of superconductivity into the magnet and to study spin splitting into the superconductor. These phenomena are investigated as a function of parameters such as temperature, magnet polarization, interfacial scattering, sample size and Fermi wavevector mismatch, all of which turn out to have important influence on the results. These comprehensive results should help characterize and analyze future data and are shown to be in agreement with existing experiments.

74.50.+r, 74.25.Fy, 74.80.Fp

I. INTRODUCTION

The importance of understanding the characteristic length scales and geometrical effects inherent to heterostructures consisting of ferromagnets in electrical contact with superconductors has received a considerable reinforcement from the ever increasing advances in nanofabrication technology. These advances have made it possible (see e.g. Refs. 1–3) to fabricate high quality nanostructures involving ferromagnets, as well as normal metals, and superconductors. In parallel, there has been significant progress in the development and refinement in tunneling spectroscopy techniques. Scanning tunneling microscopy (STM) allows one to locally probe the electronic density of states (DOS) of hybrid systems over atomic length scales with sub-meV sensitivity.

When a normal metal is in good electrical contact with a superconductor, superconductivity is weakened in the superconductor and induced in the normal metal. When the normal metal is not magnetic, this phenomenon is the traditional⁴ proximity effect which is described quantitatively via the pair amplitude, $F(\mathbf{r})$, which encompasses the spatial dependence of pair correlations in the both the superconductor and the normal metal. If the non-superconductor is a ferromagnet, the superconducting proximity effect is drastically modified by the finite exchange field. Furthermore, the magnetic material can induce spin polarization in the superconductor, resulting in a magnetic proximity effect. The study of the spatial variation of both the pair amplitude and the local DOS are fundamental to the understanding of these nanostructures.

When considering such inhomogeneous systems, there are multiple length scales involved that must be elucidated. At $T = 0$ the phase coherence in a clean normal metal in contact with a superconductor decays inversely with distance from the interface, with a characteristic length, $\xi_N(0)$, that is essentially infinite.⁵ At finite temperatures, the phase coherence decays exponentially

over a much reduced distance $\xi_N(T)$.⁴ Conversely, at low temperature, the pair correlations in the superconductor become depleted near the interface over a length scale given by the zero temperature superconducting coherence length ξ_0 , while for temperatures close to T_c , Ginzburg Landau theory⁶ predicts that the depletion is governed by a length scale $\xi_S(T)$ that diverges at T_c . Although the essentials of the standard proximity effect have been well understood for a long time,⁴ the length scales in the intermediate temperature regimes have not been systematically or consistently studied for a normal metal-superconductor bilayer system, although self consistent microscopic calculations exist for layered structures,⁷ and results within the quasiclassical⁸ description have been obtained. Other predictions are limited by being based on phenomenological or non-self consistent approaches.

If the nonmagnetic normal metal is replaced with a ferromagnet (F/S junctions and structures), the relevant length scales in the problem are altered significantly. Naively, one would expect that all phase coherence would be lost in the magnet, since the superconductor and ferromagnet have opposite types of long-range ordering: a ferromagnet favors parallel spin alignment and acts as an effective pair-breaker, while a superconductor is comprised of Cooper pairs with (in the ordinary s -wave pairing considered here) antiparallel spin alignment. However, a stable superconducting state can arise in the ferromagnet in which the Cooper pairs have a net center of mass momentum.⁹ The spin splitting in the ferromagnet introduces a new length scale ξ_2 set by the difference in the spin up and spin down Fermi wavevectors, $\xi_2 \propto (k_{F\uparrow} - k_{F\downarrow})^{-1}$, which is typically much smaller than ξ_0 .

An interesting manifestation of this effect is the π phase junction comprised of a ferromagnetic material sandwiched between superconductors.^{10–12} This particular interplay of ferromagnetism and superconductivity has been studied for some time.^{13–15} The peculiar oscillatory state (originally introduced in the context of a

new superconducting state that arises in when magnetic impurities are present^{16,17}) leads, in the sandwich geometry, to a nonmonotonic dependence of the critical temperature on the ferromagnet layer thickness.^{18–21} Other works²² have focused on the variation of the Josephson current with temperature. For certain values of the exchange field, spontaneous currents²³ may arise in F/S heterostructures.

For heterostructure configurations in which any of the material thicknesses are of order of or smaller than the largest of the relevant intrinsic lengths, size effects will play a role, and the finite thicknesses of the layers become important geometric lengths in the proximity effects. It is then clearly preferable to tackle the problem using a theory which does not involve coarse graining over atomic length scales. It has been shown that in thin superconductor-normal metal bilayers, the interlayer resistance plays a key part.²⁴ Variations in the local DOS were calculated as a function of ferromagnet thickness.^{25,26} These calculations were all based on the quasiclassical Usadel²⁷ or Eilenberger²⁸ equations. The use of quasiclassical techniques may not be appropriate when the thickness of the materials is only of a few atomic layers. Also, the Usadel equations are restricted to the limit when the mean free path is much smaller than any other relevant length scale in the problem, and therefore their use in these situations is questionable. It is therefore desirable to study finite-sized systems using a microscopic, self-consistent theory that can accurately account for these geometrical effects.

We are aware of no work that addresses the influence on the proximity effect of the mismatch between the three Fermi energies (or Fermi wave vectors) present in F/S junctions (corresponding to the superconductor, and to the up and down spin bands in the magnet). Previous work²⁹ on this question was limited to the case of nonmagnetic metal, at temperatures near T_c . It was found that when the Fermi wave vector in the normal side is smaller than that in the superconductor, a strong suppression of the pair amplitude in the normal metal ensues. Also for nonmagnetic materials, the DOS was studied⁷ using a microscopic formalism that allowed for different Fermi wavevectors, in the context of layered short-coherence length superconducting structures, but there was no systematic study. Therefore this influence is still an open question in the full parameter range. For F/S junctions, the influence of Fermi wave vector mismatches on the proximity effect is virtually uncharted territory. Spectroscopy studies³⁰ revealed a nontrivial dependence of the conductance spectrum on Fermi wave vector mismatch, however the proximity effect was ignored there and the calculation was not self consistent.

Another relevant quantity that has a strong influence on the proximity effects and which has been insufficiently studied, is the interfacial scattering strength. The variation of T_c with interface scattering strength was calculated,³¹ and the influence of interface scattering was investigated experimentally^{32,33} for $S/F/S$ structures.

High-sensitivity transport measurements³² revealed that interface barrier strength was an important parameter. It is thus desirable to study the effects of varying degrees of barrier strength on the characteristic proximity lengths. Since appreciable scattering at the interface should lead to a reduction in $F(\mathbf{r})$ near the interface, this is another example where a systematic, self-consistent solution to this problem is needed.

The main aim of this paper is therefore to present an extensive theoretical investigation of the influence of these many relevant parameters on the F/S proximity effects. We will use for these purposes a very recently developed numerical method that allows for the exact *self consistent* solution of the relevant microscopic equations. The approach is based on numerically solving the continuum Bogoliubov de Gennes (BdG) equations⁶ for the quasiparticle amplitudes. The method of numerical self consistent solution has been described in Ref. 34 where results for particular cases (zero temperature, no barrier or mismatch, and semi-infinite geometry) were given. These procedures allow for the study of coherence lengths much longer than those one can consider in lattice real-space models.^{35,36} It was shown³⁴ that for F/S junctions there is, besides the usual characteristic spatial period ξ_2 , another length scale $\xi_1 \approx \xi_2$ which describes the fast decay of $F(\mathbf{r})$ very near the interface. The above calculations were performed only at $T = 0$. Finding the temperature dependence of the F/S proximity effects will thus be a part of our task here.

Our objective is to investigate the length scales characterizing the F/S proximity effects in both bulk and finite sized junctions consisting of a ferromagnet of varying polarization, (including the nonmagnetic limit) in contact with a superconductor. As alluded to above, the often extreme differences in length scales in the problem require a self consistent microscopic theory that can deal with them simultaneously without the approximations inherent to quasiclassical and dirty-limit equations. We shall explore the whole of the parameter range including the effects of temperature, Fermi energy mismatch, interfacial scattering, and finite sample size. Results will be given for the pair amplitude and for the local DOS for both bulk and finite heterostructures, and thus we will analyze the various length scales involved.

Although the objective of this comprehensive study is to stimulate new experiments and to help analyze and characterize the resulting data, we aim also to make contact with existing experimental work. Recent STM measurements³⁷ indicate a clear modification to the normal metal density of states for a Nb-Au junction, as a function of superconductor width. We compare our results with this data using a bilayer model in which both the normal metal and superconductor have widths of order ξ_0 . We also compare our theoretical results with tunneling data³ from a F/S (Ni-Al) junction in which local DOS measurements were taken in the superconductor. The relatively large exchange energy of Ni makes it an ideal candidate for investigating the effect of magnetism

on the pairing correlations in the superconductor. In both cases, we find, using relevant values of the parameters describing the materials used and the geometry of the experimental set up, very good agreement between theory and experiment.

The rest of this paper is organized as follows. In Sec. II, we outline the method of self consistent solution to the problem. In Sec. III, we present our results for the numerous parameters discussed above for different geometries, and compare our results with recent tunnel spectroscopy data. Finally in Sec. IV we summarize our conclusions.

II. METHOD

In this section we briefly outline our basic equations and methods. We begin with a brief review of the spin dependent microscopic BdG equations in our geometry, and then outline the numerical method used for solving them. We also explain the procedure for calculating physical quantities paramount in the study of proximity effects, namely the pair amplitude and the local DOS. Most of the techniques used here follow those of Ref. 34. We will omit many of the details given there and we focus our attention below on those points where the methods employed depart from those developed in that work, such as the inclusion of an insulating barrier and of finite temperatures.

The BdG equations⁶ are a conceptually simple and convenient set of microscopic equations used for studying inhomogeneous superconducting systems, in our case structures involving, in addition to the superconductor, a ferromagnet or a non-magnetic normal metal. We consider a particular slab-like geometry where the materials are assumed to extend to infinity in the $x - y$ plane, and have a total arbitrary thickness d along the z direction, where the only geometrical variation occurs. We denote the thicknesses of the ferromagnetic and superconducting layers by d' and $d - d'$ respectively. These materials are in general separated by a thin insulating barrier at $z = d'$. Since in this geometry the system is translationally invariant in the $x - y$ plane, some aspects of the problem are effectively one-dimensional. For this configuration, we then have two sets of coupled equations, one for the spin-up and spin-down quasiparticle and quasihole wave functions $(u_n^\uparrow, v_n^\downarrow)$, and another for $(u_n^\downarrow, v_n^\uparrow)$. The first takes the form^{6,34} ($\hbar = k_B = 1$),

$$\left[-\frac{1}{2m} \frac{\partial^2}{\partial z^2} + \varepsilon_\perp + U(z) - E_F(z) - h_0(z) \right] u_n^\uparrow(z) + \Delta(z) v_n^\downarrow(z) = \epsilon_n u_n^\uparrow(z), \quad (1a)$$

$$-\left[-\frac{1}{2m} \frac{\partial^2}{\partial z^2} + \varepsilon_\perp + U(z) - E_F(z) + h_0(z) \right] v_n^\downarrow(z) + \Delta(z) u_n^\uparrow(z) = \epsilon_n v_n^\downarrow(z), \quad (1b)$$

where ε_\perp is the transverse kinetic energy, ϵ_n are the quasiparticle energy eigenvalues (the index n labels the

relevant quantum numbers), $h_0(z) = h_0 \Theta(z - d')$ is the magnetic exchange energy. Scattering at the interface (assumed to be spin independent) is accounted for by the potential $U(z) = H \delta(z - d')$, where H is the barrier strength parameter. The pair potential $\Delta(z)$ satisfies a self-consistency condition as discussed below, and since we will assume that there is no current flowing in the system, we can take it to be real. In general, we must allow for the possibility of having up to three different Fermi wavevectors or band widths³⁰ in the problem. The quantity $E_F(z)$ equals E_{FM} in the magnetic side, $0 < z < d'$, so that $E_{F\uparrow} = E_{FM} + h_0$, and $E_{F\downarrow} = E_{FM} - h_0$, while in the superconducting side, $d' < z < d$, $E_F(z) = E_{FS}$. We will be assuming parabolic bands so that $\varepsilon_\perp = 1/2m(k_x^2 + k_y^2)$ and there are three Fermi wave vectors, corresponding to $E_{F\uparrow}$, $E_{F\downarrow}$ and E_{FS} . The solutions for the other set of wavefunctions $(u_n^\downarrow, v_n^\uparrow)$ are easily obtained from those of Eqns. (1) by allowing for both positive and negative energies, and then using the transformation: $u_n^\uparrow \rightarrow v_n^\uparrow, v_n^\downarrow \rightarrow -u_n^\downarrow, \epsilon_n \rightarrow -\epsilon_n$.

Equations (1) must be solved in conjunction with the self consistency condition for the pair potential,

$$\Delta(z) = \frac{g(z)}{2} \sum_n' [u_n^\uparrow(z) v_n^\downarrow(z) + u_n^\downarrow(z) v_n^\uparrow(z)] \tanh(\epsilon_n/2T), \quad (2)$$

where T is the temperature, and $g(z)$ is the effective BCS coupling constant, which will be taken to be zero outside the superconductor and a constant within it. The prime on the sum in (2) indicates that the sum is restricted to eigenstates with $|\epsilon_n| \leq \omega_D$, where ω_D is the Debye energy.

We now solve Eq. (1) by expanding the quasiparticle amplitudes in terms of a complete set of functions $\phi_q(z)$,

$$u_n^\uparrow(z) = \sum_q^N u_{nq}^\uparrow \phi_q(z), \quad v_n^\downarrow(z) = \sum_q^N v_{nq}^\downarrow \phi_q(z). \quad (3)$$

We will use the normalized particle in a box wavefunctions, $\phi_q(z) = \sqrt{2/d} \sin(k_q z)$, as our choice for the complete set. Here $k_q = q/\pi d$, and q is a positive integer. The finite range of the pairing interaction ω_D permits the sums in (3) to be cutoff at an integer N as discussed in Ref. 34, in a way that depends on the maximum wavevector present. Upon inserting the expansions (3) into (1), and making use of the orthogonality of the $\phi_q(z)$, we arrive at the following $2N \times 2N$ matrix eigensystem,

$$\begin{bmatrix} H^+ & D \\ D & H^- \end{bmatrix} \Psi_n = \epsilon_n \Psi_n, \quad (4)$$

where Ψ_n is the column vector corresponding to $\Psi_n^T = (u_{n1}^\uparrow, \dots, u_{nN}^\uparrow, v_{n1}^\downarrow, \dots, v_{nN}^\downarrow)$. The matrix elements are given by

$$H_{qq'}^+ = \left[\frac{k_q^2}{2m} + \varepsilon_\perp \right] \delta_{qq'} + \int_0^d dz \phi_q(z) U(z) \phi_{q'}(z)$$

$$-E_{F\uparrow} \int_0^{d'} dz \phi_q(z) \phi_{q'}(z) - E_{FS} \int_{d'}^d dz \phi_q(z) \phi_{q'}(z), \quad (5a)$$

$$H_{qq'}^- = - \left[\frac{k_q^2}{2m} + \varepsilon_{\perp} \right] \delta_{qq'} - \int_0^d dz \phi_q(z) U(z) \phi_{q'}(z)$$

$$+ E_{F\downarrow} \int_0^{d'} dz \phi_q(z) \phi_{q'}(z) + E_{FS} \int_{d'}^d dz \phi_q(z) \phi_{q'}(z), \quad (5b)$$

$$D_{qq'} = \int_{d'}^d dz \phi_q(z) \Delta(z) \phi_{q'}(z). \quad (5c)$$

The self-consistency condition is now transformed into,

$$\Delta(z) = \frac{g(z)}{2} \sum_{p,p'} \sum_n' \tanh(\varepsilon_n/2T) \times$$

$$\left[u_{np}^{\uparrow} v_{np'}^{\downarrow} \phi_p(z) \phi_{p'}(z) + u_{np}^{\downarrow} v_{np'}^{\uparrow} \phi_p(z) \phi_{p'}(z) \right]. \quad (6)$$

where the sum over the quantum numbers n encompasses a sum over the continuous transverse energy ε_{\perp} and a quantized longitudinal momentum index q ,

$$\sum_n' \rightarrow \sum_{\varepsilon_{\perp}}' \sum_q'. \quad (7)$$

The matrix eigensystem Eqn. (4) and the self-consistency condition (6) constitute the primary equations drawn upon in this paper. They are solved numerically, using the algorithm developed and described in previous work³⁴. The iterative computational process is completed when the maximum relative error in $\Delta(z)$ between successive iterations is less than a prescribed value as explained below.

Once we have the self-consistently calculated eigenvalues and eigenvectors, we can then construct all relevant physical quantities. For example, the usual penetration depths are conveniently obtained from the pair amplitude $F(z)$,

$$F(z) = \Delta(z)/g(z). \quad (8)$$

The pair amplitude, unlike $\Delta(z)$, is therefore not restricted by the coupling constant to vanish in the non-superconductor. $F(z)$ gives a quantitative measure of the superconducting correlations in both the superconductor and non-superconductor where there may exist phase coherence between particle and hole wave functions. The value of $F(z)$ in the non-superconducting region however, does not affect the quasiparticle dynamics since it is only $\Delta(z)$ that enters into the BdG equations.

We can also use our numerical results for the excitation spectra to calculate the experimentally accessible local single particle properties via the thermally broadened density of states (DOS)

$$N(z, \varepsilon) = N_{\uparrow}(z, \varepsilon) + N_{\downarrow}(z, \varepsilon), \quad (9)$$

where the local DOS for each spin state is given by,³⁸

TABLE I. Dimensionless variables

Physical quantity	Dimensionless form
Exchange energy	$I \equiv h_0/E_{FM}$
Fermi wavevector mismatch	$\Lambda \equiv (k_{FM}/k_{FS})^2$
Temperature	$t \equiv T/T_c$
Coherence length	$\Xi_0 \equiv k_{FS}\xi_0$
Debye energy	$\omega \equiv \omega_D/E_{FS}$
Barrier strength	$H_B \equiv mH/k_{FM}$
Distance relative to interface	$Z \equiv k_{FS}(z - d')$

$$N_{\uparrow}(z, \varepsilon) = - \sum_{p,p'} \sum_n' [u_{np}^{\uparrow} u_{np'}^{\uparrow} \phi_p(z) \phi_{p'}(z) f'(\varepsilon - \varepsilon_n)$$

$$+ v_{np}^{\uparrow} v_{np'}^{\uparrow} \phi_p(z) \phi_{p'}(z) f'(\varepsilon + \varepsilon_n)], \quad (10a)$$

$$N_{\downarrow}(z, \varepsilon) = - \sum_{p,p'} \sum_n' [u_{np}^{\downarrow} u_{np'}^{\downarrow} \phi_p(z) \phi_{p'}(z) f'(\varepsilon - \varepsilon_n)$$

$$+ v_{np}^{\downarrow} v_{np'}^{\downarrow} \phi_p(z) \phi_{p'}(z) f'(\varepsilon + \varepsilon_n)]. \quad (10b)$$

Here $f'(\varepsilon) = \partial f/\partial \varepsilon$ is the derivative of the Fermi function. We will also be interested in the quantity

$$\delta N(z, \varepsilon) = N_{\uparrow}(z, \varepsilon) - N_{\downarrow}(z, \varepsilon), \quad (11)$$

which will be used to characterize the effective leakage of magnetism into the superconductor.

III. RESULTS

In this Section, we present numerical results for the pair amplitude and local DOS, and discuss other physically meaningful quantities arising from the self consistent excitation spectra. We will analyze the various length scales characterizing the influence of the superconductor on the ferromagnet and vice versa. Since we will consider systems with a wide range of superconductor and ferromagnet widths and physical parameters, we divide this section into four different subsections dealing with the following topics: (1) systematics of the temperature, exchange field, Fermi wave vector mismatch and barrier height for bulk F/S systems. (2) dependence of the results on the finite thickness of either the F or the S layer, and finally (3) a comparison with experimental results.

Most of the results are conveniently expressed in terms of the dimensionless quantities compactly defined and listed in Table I. Unless otherwise indicated, we use $\omega = 0.1$ for the Debye cutoff in units of E_{FS} and $\Xi_0 \equiv k_{FS}\xi_0 = 50$ in this work. All lengths z are measured in units of the inverse of k_{FS} . For example the widths of the ferromagnet or superconductor layers are represented as, $D_F = k_{FS}d'$, and $D_S = k_{FS}(d - d')$. The bulk case is studied by choosing values of D_S and D_F sufficiently large so that the results become independent of these quantities.

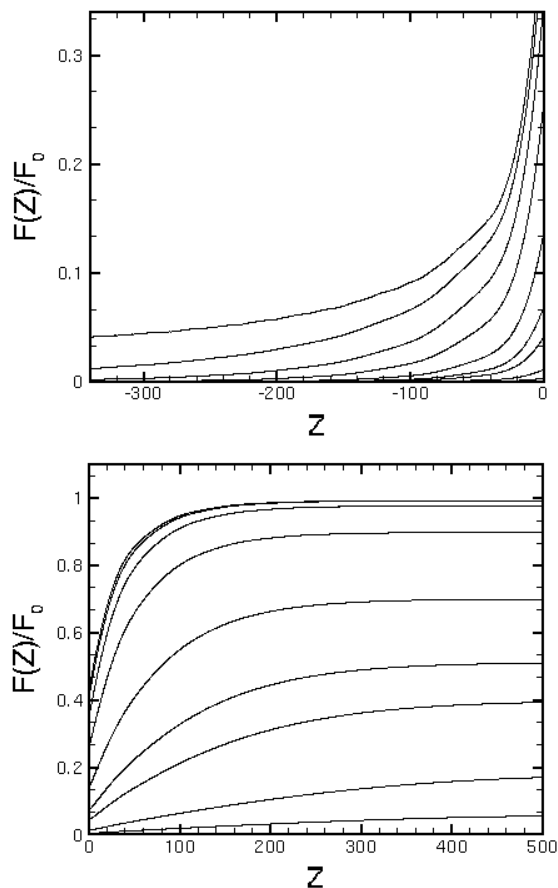


FIG. 1. The pair amplitude $F(z)$, normalized to the zero T bulk value $F_0 = \Delta_0/g$ in the superconductor, plotted as a function of dimensionless distance $Z = k_{FS}z$ from the interface. The top panel depicts the normal metal ($I = 0$) region, while the bottom panel shows the superconducting region. In both cases the curves correspond, from top to bottom, to temperatures $t \equiv T/T_c = 0, 0.2, 0.4, 0.6, 0.8, 0.9, 0.94, 0.98, 0.99$. Note the different vertical and horizontal scales used in both panels.

As mentioned above, we employ a numerical algorithm as in Ref. 34 to solve the self consistent eigenvalue problem Eqns. (4), (6). The procedure involves making a reasonable initial guess for $\Delta(z)$, where the coordinate z is of course discretized for numerical purposes. The initial guess may be taken to be a previously obtained converged result corresponding to a slightly different set of parameter values, or, in the absence of any such suitable previous result, a step function, e.g., $\Delta(Z) = \Delta_0\Theta(Z)$, where Z is the dimensionless distance from the interface (see Table I), and Δ_0 the bulk value of the gap at $T = 0$. We then diagonalize the $2N \times 2N$ matrix described by Eqn. (4) for each value of ε_{\perp} . The cutoff number N , as explained in Ref. 34 depends chiefly on $D \equiv k_{FX}d$, where k_{FX} is the largest Fermi wavevector in the problem and d the total thickness, which is up to $1200k_{FS}^{-1}$ in our calculations. We use 5000 different values of ε_{\perp} consistent with the

energy cutoff. The value 5000 is five to ten times larger than that used in previous work, which makes for better convergence and smoother results. Self consistency is achieved³⁴ via an iteration process. The process terminates when the relative error between successive $\Delta(z)$ is less than a suitable number, chosen here to be 10^{-4} (one tenth of the criterion in previous work). The pair potential settles down, after starting with a step function initial guess, to its self-consistent form within about twenty five iterations. This value is typical for most parameter values and system sizes used in this paper. The only exceptions are when the temperature approaches T_c (the bulk transition temperature of the superconductor), or when the superconductor width is of order of ξ_0 . Then the number of iterations needed for self-consistency is much larger (up to several hundred) if one starts with a step function guess for $\Delta(Z)$. This problem can be alleviated by calculating $\Delta(z)$ self-consistently for a given temperature and then use this as input for a nearby temperature as described above.

A. Systematics of the Parameter Dependence

We consider in this Subsection the dependence of the results on temperature and on material parameters (exchange field, wave vector mismatch and barrier height), in the limit where both ferromagnet and superconductor are very thick (“bulk” limit). By this we mean that both D_F and D_S are taken to exceed the temperature dependent BCS coherence length. In this subsection we have taken $D_F = D_S = 12\Xi_0$ (recall $\Xi_0 = 50$), so that $D_F, D_S \gg \Xi_0$ and we are in the bulk limit except extremely close to T_c , $t \lesssim 0.99$. We subdivide the analysis into three categories that address respectively temperature and exchange effects, Fermi energy mismatch, and interfacial scattering effects.

1. Temperature and exchange energy dependence

We now consider how variation of the temperature affects the pair amplitude and local DOS for select values of the dimensionless exchange energy I . To isolate these effects, we assume that there is no interface barrier and no Fermi energy mismatch ($\Lambda = 1$, $H_B = 0$, see Table I). We first examine the case where the non-superconductor is a normal metal ($I = 0$). In Fig. 1, the pair amplitude $F(Z)$ is shown in the normal metal and superconductor sides respectively for a wide range of temperatures. In all plots, we normalize $F(Z)$ to the zero T bulk value $F_0 = \Delta_0/g$. The two regions $Z > 0$ (superconductor) and $Z < 0$ (normal) are plotted in separate panels because their significant features occur over different length and vertical scales. The pair amplitude however, is continuous across the interface. We see that in the normal

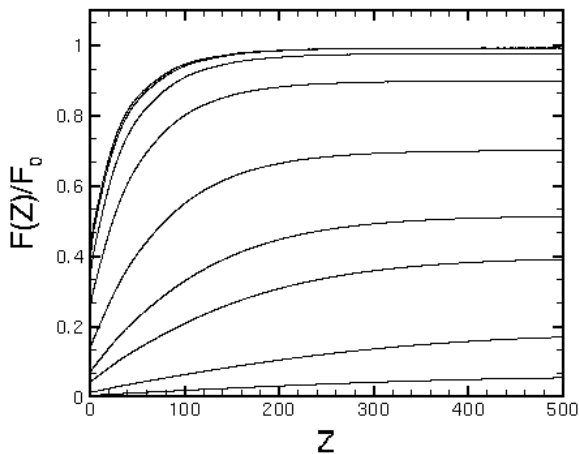
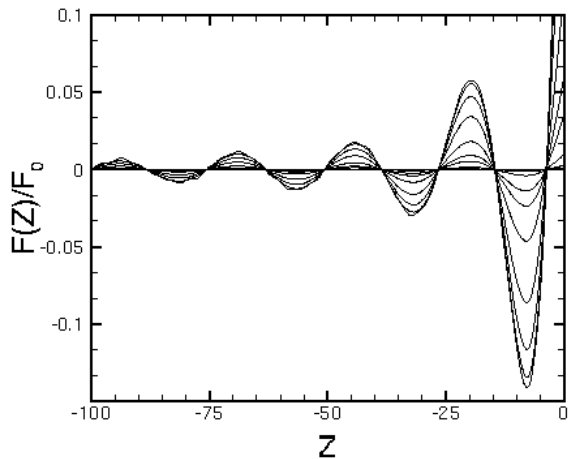


FIG. 2. Normalized pair amplitude as a function of distance, in both the ferromagnetic (top panel) and the superconducting side (bottom panel), at the same temperatures as in Fig. 1. The data is for $I = 1/4$, with all other parameters as in Fig. 1. In the top panel, the amplitude of the oscillations decays monotonically with increasing t .

metal, Fig. 1 (upper panel), $F(Z)$ has a different functional form at zero temperatures (top curve) than at finite temperatures. At $T = 0$ $F(Z)$ has a very slow decay into the normal region, and is expected⁵ to decay as the inverse of the distance from the interface,

$$F(Z) = \frac{c_1}{|Z| + c_2}, \quad (12)$$

where c_1 and c_2 are constants. We find that the expression Eqn. (12) is valid, but only in a fairly narrow range close to the interface. The actual behavior over the range shown is more complex, which reflects that the decay of $F(Z)$ takes place, as we shall see, over two length scales. Upon increasing T , thermal effects reduce the phase coherence of the electron-hole wavefunctions and the relevant length scale in the normal metal is set by⁴

$$\xi_N(T) = v_{FM}/2\pi T. \quad (13)$$

where $v_{FM} \equiv k_{FM}/m$. It is clear from the top panel of Fig. 1 that as T increases the length scale character-

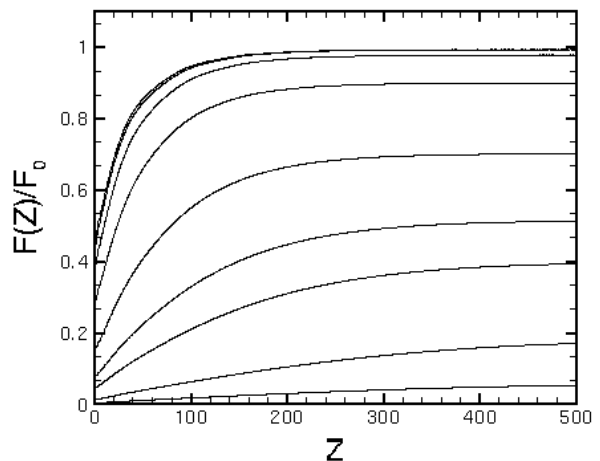
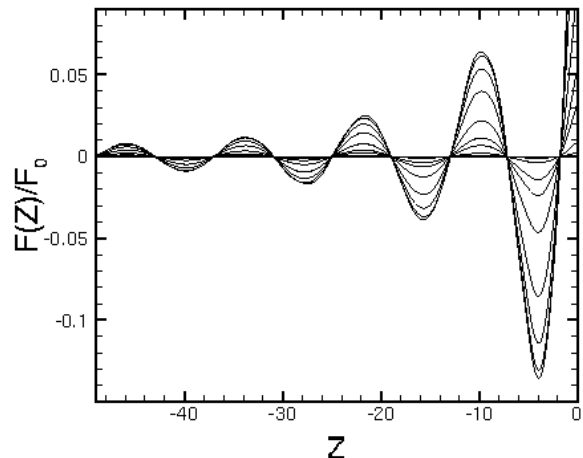


FIG. 3. Normalized pair amplitude for $I = 1/2$, plotted as in Fig. 2, for the same parameter values and temperatures. Note the reduction in the characteristic period compared to Fig. 2.

izing the decay of $F(Z)$ decreases. The decay of $F(Z)$ at a fixed, finite temperature cannot be fit to a single exponential in all of the spatial region shown. For temperatures close to T_c , and far from the interface, an approximate form for the pair amplitude has been given,⁴

$$F(Z) = \Phi(Z) \exp(-|Z|/\xi_N(T)), \quad (14)$$

where $\Phi(Z)$ is a slowly varying function. Our results agree with Eqn. (14) in the temperature regime near T_c ($t > 0.9$), and for sufficiently large $|Z|$. ($|Z| > \Xi_0$). However, the overall decay of $F(Z)$ is more complicated and cannot be described by a single exponential decay. There always seems to be a second length scale in the problem, even near T_c .

Turning now to the superconductor side, the lower panel of Fig. 1 shows the normalized pair potential $F(Z)$ at the same values of T used in the panel above it. At $T = 0$, the characteristic decay length of the pair amplitude is given by the usual zero temperature BCS coherence length ξ_0 . As the temperature is increased however,

the depletion of superconducting correlations occur over a length scale which increases with T . We denote this scale (in units of inverse k_{FS}) by $\xi_S(T)$. For temperatures close to T_c the profile for the pair amplitude is well known from standard Ginzburg-Landau theory⁶, and has the following form

$$F(Z) = F_0(T) \tanh \left[\frac{Z + Z_0}{\sqrt{2} \xi_S(T)} \right], \quad (15)$$

where Z_0 is a parameter to be determined by the condition

$$\left(\frac{1}{F} \frac{dF}{dz} \right)_{z=0} = \frac{1}{b}, \quad (16)$$

and b is an extrapolation length, which in our dimensionless units is of order Ξ_0^2 . These expressions hold provided³⁹ that Ξ_0 is not too small. Our results fit Eq.(15) adequately for temperatures $T \lesssim T_c$ over the entire Z range shown. As the temperature is decreased, the expression in Eqn. (15) ceases to be correct for the entire range of Z , but remains an adequate fit within a region of at least one coherence length from the interface. We use this expression, therefore as a fitting function even at lower temperatures in order to extract the dimensionless length scale ξ_S characterizing the decay away from the interface. We find that for most of the temperature range, the characteristic length ξ_S fits well to the Ginzburg-Landau expression

$$\xi_S(T) = 0.74 \Xi_0 \left(\frac{1}{1-t} \right)^{1/2}. \quad (17)$$

After having shown the dependence of $F(z)$ on intermediate temperatures $0 < T \lesssim T_C$ for $I = 0$, and having verified that our limiting results are in agreement with previous theory and expectations for the standard (non-magnetic) proximity effect, we turn to the more interesting case where the exchange energy parameter I is finite. We found above that when $I = 0$, the superconducting correlations extend well within the normal metal at $T = 0$, but decay more rapidly as the temperature is increased. When an exchange field is present, the spin degeneracy that existed for $I = 0$, is removed. The result is that the Fermi wave vectors of the spin up and spin down electrons, $k_{F\uparrow}, k_{F\downarrow}$, are different, and consequently a Cooper pair entering the ferromagnet acquires a net center of mass momentum. The superconducting order induced in the ferromagnet arises from the product of particle and hole wave functions (e.g., $u_n^\dagger(z)v_n^\dagger(z)$) summed over all quantum numbers n . It is the superposition of these wavefunctions that causes the superconducting wavefunction to oscillate⁹ on a length scale set by the difference in the spin up and spin down wave vectors, $\xi_2 \approx (k_{F\uparrow} - k_{F\downarrow})^{-1}$. We have

$$k_{FS}\xi_2 = \frac{1}{(\Lambda(1+I))^{1/2}} k_{F\uparrow}\xi_2 \quad (18)$$

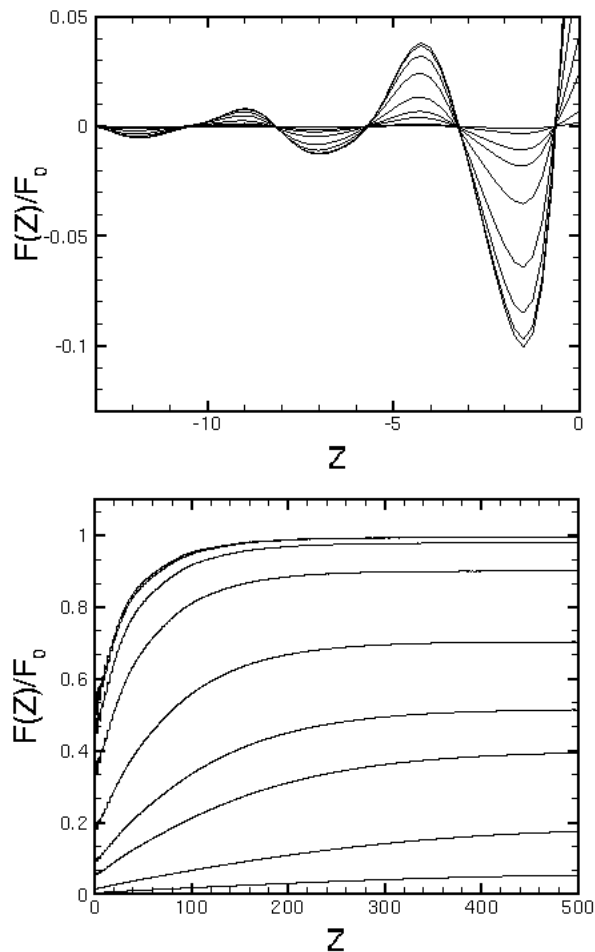


FIG. 4. Normalized pair amplitude for $I = 1$, plotted as in Figs. 2 and 3, for the same parameter values and temperatures. Note the deviation from the simple sinusoidal decay of Eqn. 20 on the magnetic side.

where Λ is the wavevector mismatch parameter of Table I. Since³⁴ $k_{F\uparrow}\xi_2 \approx 1/I$, we see that the characteristic length of oscillations scales as $1/I$, and therefore, except at extremely small I , it is much smaller than length scale set in the normal metal case above.

We have previously studied³⁴ the explicit form for the pair amplitude in the ferromagnet at zero temperature. We found that for most exchange fields, and except extremely near the the interface, the pair amplitude is given by

$$F(Z) = \alpha \frac{\sin[Z/(k_{FS}\xi_2)]}{(Z/(k_{FS}\xi_2))}, \quad T = 0, \quad (19)$$

where α is a constant. Very close to the interface, the pair amplitude monotonically decays over a characteristic length ξ_1 which is defined as the first point inside the ferromagnet at which $F(Z)$ is zero. The length scale ξ_1 goes also as $k_{FS}\xi_1 \approx 1/I$.

We are interested in how the pair amplitude and various characteristic lengths associated with it are modified as T increases, at finite I . We therefore display in

Fig. 2 the pair amplitude at both the ferromagnet and superconductor for $I = 1/4$ and the same temperature values used in Fig. 1. As in that case, the split panel arrangement is required by the difference in vertical and horizontal scales, but the function $F(Z)$ is always continuous at the interface. We focus first on the ferromagnetic region. Starting with the top curve in the upper panel of Fig. 2 ($T = 0$), we see that, beyond a small region of fast decay at the interface, the pair amplitude exhibits damped oscillations, with a temperature independent period that coincides with the expected value $k_{FS}\xi_2 \approx 1/I = 4$, independent of T . The envelope decay of the oscillations varies inversely with distance as given in Eqn. (19). The quantity ξ_1 is also independent of temperature, since as can be seen in the Figure, the location of the first node of $F(Z)$ as it monotonically goes to zero near the interface is the same for all temperatures. As T increases, however, the amplitude of the oscillations in $F(Z)$ markedly decreases. This decrease, as we shall see below, is not merely a reflection of the smaller value of $\Delta(T)$ in the bulk superconductor. Because of this competition between thermal and exchange energies, the pair amplitude now has a slightly more complicated functional form than that given by Eqn. (19). We find that in order to fit our numerical results, Eqn. (19) must be modified by incorporating additional spatial and temperature dependent factors. The amplitude of the oscillatory decay of $F(Z)$ no longer decays as the inverse distance from the interface, but now has an additional slowly varying exponential term $\Phi'(Z)$, and a purely temperature dependent amplitude, $A(t)$,

$$F(Z) = A(t)\Phi'(Z)\frac{\sin[(Z+\theta)/k_{FS}\xi_2]}{(Z+\theta)/k_{FS}\xi_2}, \quad (20)$$

where θ is a small, weakly I dependent shift that accounts for the sharp monotonic decay right at the interface into the ferromagnet. We find that Eqn. (20) holds for nearly the entire range values of I $0 \leq I \leq 1$. Certain exceptions occur in the extreme cases of very small $I \simeq \Delta_0/E_{FM}$ or very large $I \simeq 1$ and will be addressed below. The temperature dependence of the amplitude $A(t)$ in Eqn. (20), is fitted well by the form $A(t) = A(0)(1-t^2)$. Thus $A(t)$ decreases faster with temperature than the bulk $\Delta(T)$, which shows that the decrease of the amplitude with temperature is not merely a normalization effect but involves an intrinsic decrease of the pairing at the interface. Temperature has a marked effect on the amplitude, but it does *not* wash out the oscillations themselves, which remain quite well defined even at temperatures quite close to T_c .

The superconductor side (bottom panel of Fig. 2) shows a behavior of $F(Z)$ very similar to that found in the $I = 0$ case, with the variation of $F(Z)$ again occurring over the length scale $\xi_S(T)$. The effect of the the exchange field on $F(Z)$ in the superconductor region therefore seems to be minimal at all temperatures. We will see below however, that the pair amplitude is

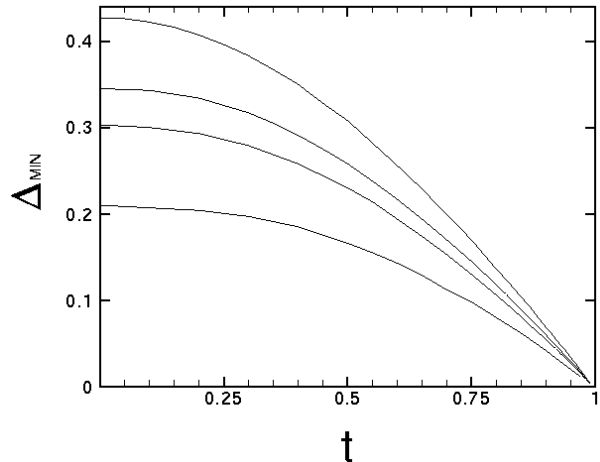


FIG. 5. Variation of the minimum value of the self consistent pair potential (Δ_{MIN}) in the superconductor as a function of dimensionless temperature for (from top to bottom) $I = 0, 0.25, 0.5, 1$.

only partially useful in conveying the total effect of magnetism leakage into the superconductor. The quantity $\delta N(z)$ from Eqn. (11) will be used below for extracting additional useful information on this question.

Continuing with larger values of I , Fig. 3 shows the case of $I = 1/2$. We first address the ferromagnet side in the top panel. $F(Z)$ follows the form given in Eqn. (20), with a damped oscillatory behavior similar to that in the $I = 1/4$ case. However, one should note in making the comparison that the horizontal axis scale here has been reduced by a factor of two with respect to that in Fig. 2 since the characteristic period has approximately halved in accordance with Eqn. (18). In the superconductor side (Fig. 3, bottom panel), the decay away from the interface is governed by the length $\xi_S(T)$. The very slight wiggles in $F(Z)$ which may be observed near the interface are due to the increased mismatch of the two Fermi energy levels in the ferromagnet with E_{FS} . Overall however, the superconducting region shows little change compared to the previous case.

We now turn to the extreme (half metallic) case of $I = 1$, where only one spin band is present in the ferromagnet at the Fermi level. We plot results in the same way, and for the same temperatures as in Figures 1, 2, and 3. The top panel in Fig. 4 illustrates the pair amplitude in the ferromagnet. The characteristic length scale that describes the main oscillatory behavior is given from Eqn. (18) as $k_{FS}\xi_2 = 1/\sqrt{2}$, (recall that we are using $\Lambda = 1$ in this subsection). The relevant spatial variations occur now only on an atomic scale, (see horizontal axis). This reflects that Andreev processes are inhibited by the absence of Fermi level down states deep within the magnet. We also see clear deviations from the pure damped sinusoidal behavior seen for the previous two exchange field values. The superconducting region (bottom panel) follows the same pattern as the other cases, but

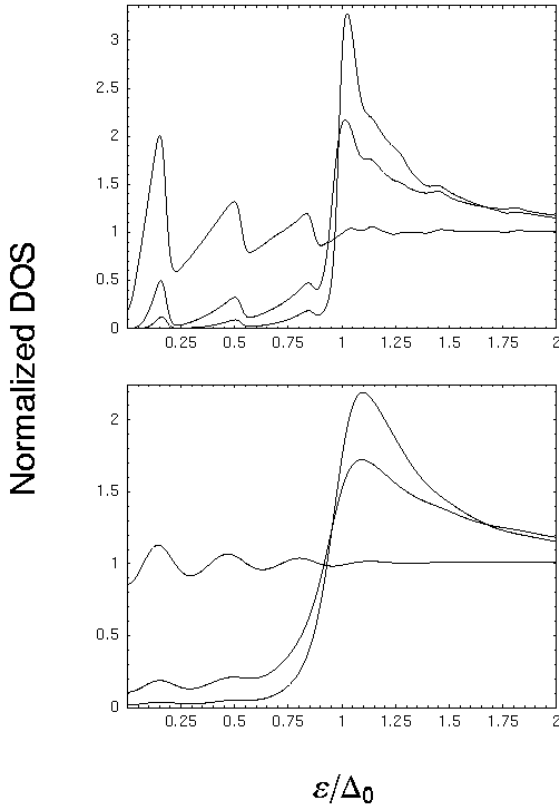


FIG. 6. Local DOS (normalized to its Fermi level value in the normal state of the superconductor) versus the dimensionless energy ϵ/Δ_0 at $I = 0$ for $t = 0.02$ (top panel) and $t = 0.1$ (bottom panel). The curves shown, from top to bottom at $\epsilon/\Delta_0 < 1$, are for for $Z = -100, 100, 200$ respectively.

here we see that very near the interface there exist small oscillations of order of the Fermi wavelength. The oscillations were barely glimpsed at $I = 1/2$ and disappear with decreasing I .

The pair amplitude at the interface at constant temperature decreases markedly with I , while at constant I it decreases with T . We illustrate this in Fig. 5, where Δ_{MIN} is the minimum value of the normalized $\Delta(Z)$ in the superconductor. This minimum occurs right at the interface, and because of the relatively wide horizontal scale in the bottom panels of Figs. 1, 2, and 3, it is not really possible to read its value from these Figures. We see in this Figure that the effect of the exchange field is quite pronounced, and that as the temperature approaches T_c , all curves tend to collapse into a nearly straight line tending to zero. The depletion of superconducting correlations with exchange field at the interface is also quite evident from the data shown.

Having studied the spatial dependence of the superconducting correlations, it is now pertinent to examine the local density of states at various positions on both sides of the interface. The local DOS gives further direct insight into the proximity effect, and more important, it is an experimentally accessible quantity. Its calcula-

tion is achieved through Eqn. (9) and the computed self consistent spectra.

We again consider first the case $I = 0$. The top panel in Fig. 6 shows the normalized (all results for the DOS in this work are presented normalized to the superconductor's normal state DOS at the Fermi level) local DOS at $t = 0.02$, while the panel below it corresponds to $t = 0.1$. For both cases the numerical results are plotted for the local DOS at the positions $Z = -2\Xi_0, 2\Xi_0, 4\Xi_0$ that is, one position in the normal metal and two in the superconductor. Focusing on the very low temperature case, (top panel), we consider first the normal metal region at $Z = -100$ (top curve in the subgap region). We see there the sawtooth-like pattern characteristic of the de Gennes-St. James states as predicted long ago⁴⁰. The DOS is small but finite at the Fermi energy due to filling by thermally excited quasiparticles, and then rises nearly linearly at small energies. The Andreev bound states are illustrated by the peaks in the DOS. These are due to constructive interference of the electron and hole wavefunctions, as they undergo Andreev reflection at the F/S interface and normal reflection at the vacuum-normal metal interface at the opposite end of the sample. The characteristic energy E_c of the peaks is determined by adding up the phases for a given trajectory⁴¹. It can be seen that, in agreement with theoretical expectations, the first peak occurs at an energy $E_c \approx \pi v_{FM}/4d' \approx 0.2\Delta_0$, while the other peaks occur approximately at multiples of $2E_c$. The energy scale E_c can be seen directly in the calculated self-consistent spectrum.⁴² In the energy region below the gap ($\epsilon/\Delta_0 < 1$), we find that for nearly longitudinal momenta ($\epsilon_{\perp} \approx 0$), there exists roughly three excitation branches, at the same energies as the peaks seen in the upper panel of Fig. 6. These peaks subsequently broaden due to the numerous quasiparticle states with momenta nearly perpendicular to the interface. The two other curves in the top panel of Fig. 6 correspond to points in the superconductor at $Z = 2\Xi_0$ and $Z = 4\Xi_0$. The bound states clearly flatten out as one moves further into the superconductor, and there are no longer any states at the Fermi energy. The BCS gap becomes quite evident at the position $Z = 4\Xi_0$, when only a hint of nonvanishing DOS can be seen at energies below Δ_0 .

Increasing the temperature tends to smear the previous lower T results. Figure 6 (bottom panel) illustrates this for the case of $t = 0.1$, and the same positions as the panel above it. In the normal metal, the sharp pronounced zig-zap pattern is now smoothed into a series of humps. The same is true for the DOS in the superconductor, where thermal excitations fill regions inside the gap, while flattening and spreading out the smoothed BCS peaks.

We now can proceed to study the effects of a finite exchange field I on the local DOS in the superconductor and ferromagnet. We begin with the ferromagnet region at $I = 1/2$, and $t = 0.02$. As already seen in Ref. 34, the effect of I on the local DOS is very drastic. The bound state phenomena in the normal side relatively far from

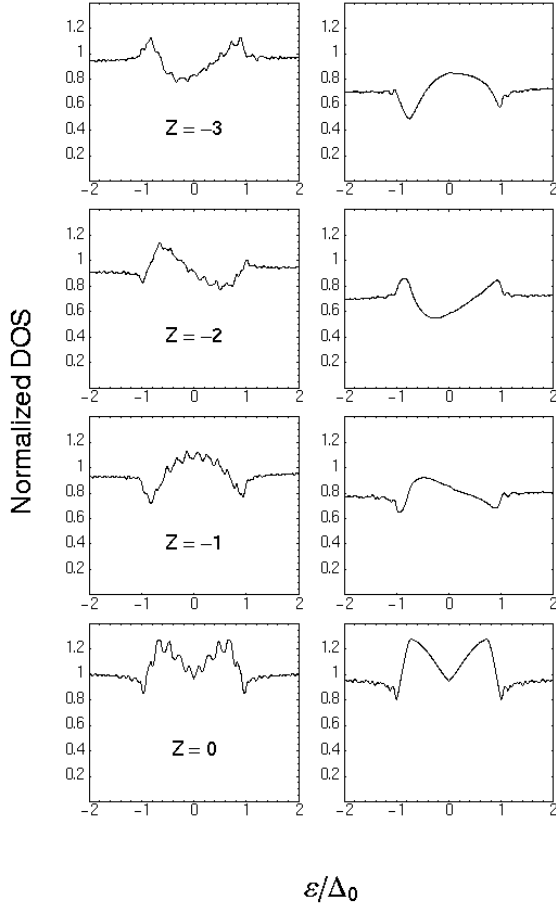


FIG. 7. Local DOS (normalized as in Fig. 6) in the ferromagnet for $I = 1/2$ and $t = 0.02$ (left column) at four positions near the interface. The right column corresponds to $I = 1$ and the same temperature and positions used in the left column.

the interface are no longer observable at $I = 1/2$ because the overall decay of superconducting correlations takes place over considerably smaller distances. On the other hand, this decay takes place now in a nonmonotonic manner, which gives rise to a new set of features in the ferromagnet, very near the interface: in the left column of Fig. 7 we show the (normalized) DOS at four positions at and very near the interface. The influence of the oscillatory pair amplitude (Fig. 3) becomes evident as we examine the four plots in this column. The subgap structure in the top curve ($Z = -3$) evolves so that maxima and minima become reversed at $Z = -1$, closer to the interface. Comparing with Fig. 3, we see that the oscillating superconducting order has in effect induced oscillations in the local DOS as a function of position within the ferromagnet, and that the large exchange field induces noticeable particle-hole asymmetry. The length scale at which the DOS flips coincides with the characteristic distance $k_{FS}\xi_2$, given in Eqn. (18). The first and third panels in Fig. 7 (left) are separated by $\Delta Z = 2$. Although this Figure depicts results obtained

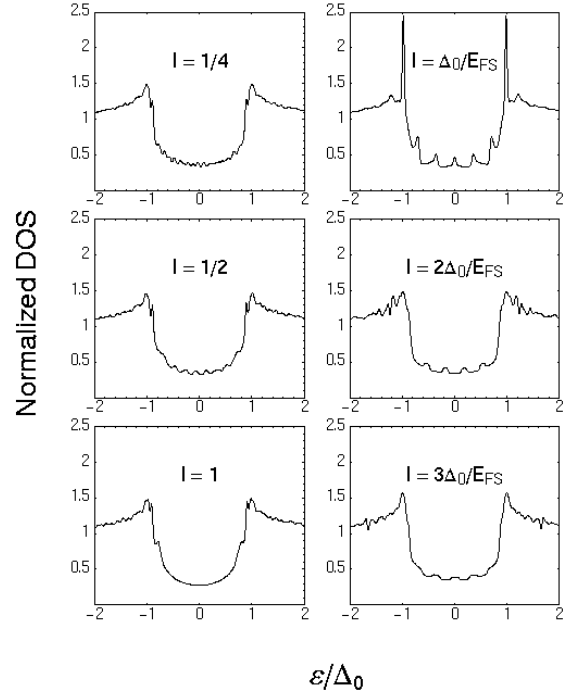


FIG. 8. Normalized local DOS at $Z = \Xi_0$ in the superconductor and $t = 0.02$ for various exchange fields as labeled in each panel. The left column corresponds to intermediate and large exchange fields, and the right column to small values of I as indicated.

for a rather low temperature, the oscillatory behavior is never completely washed out by the temperature, as remarked above in conjunction with the discussion of $F(Z)$.

The same behavior holds true *a fortiori* in the right column of Fig. 7, which displays data for the half-metallic case $I = 1$, at the same temperature and locations. One important difference between this and the left column is the spatial scale at which the DOS oscillations should occur. Since $1/I = 1$, the complete DOS inversion should occur at points separated by an interval δZ of order unity. Indeed, the curves in the right column of Fig. 7 reflect this.

In Fig. 8 we consider the superconductor side of the junction. In the left column we illustrate the local DOS one coherence length ξ_0 from the interface for three different exchange fields ranging from $I = 1/4$ to $I = 1$, at temperature $t=0.02$. In the top panel ($I = 1/4$) there is a wide U-shape opening for energies $|\epsilon/\Delta_0| < 1$. The opening then starts to get smaller and the curve trends upwards for $I = 1/2$, as seen in the middle plot of this left column. There is also a slight decrease in the number of states at the Fermi level ($\epsilon = 0$). These results are consistent with those previously obtained³⁴ at zero temperature. For the half-metallic case $I = 1$, the left bottom panel shows a further slight reduction in states at $\epsilon/\Delta_0 = 0$, but there is barely a hint of the asymmetry found in the ferromagnetic side.

It is of interest also to study the case where the ex-

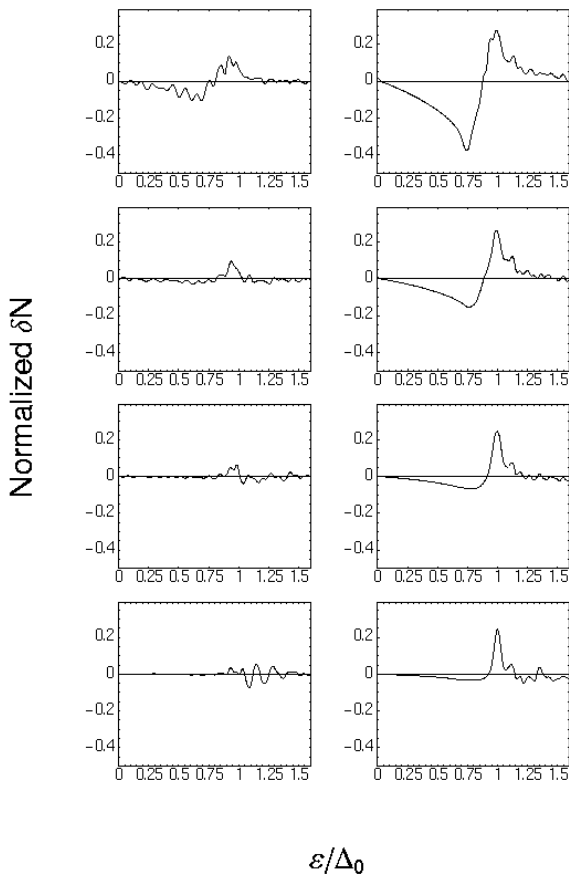


FIG. 9. δN (normalized to the normal state DOS summed over spins) in the superconductor for $I=0.25$ (left column) and $I=1$ (right column) at $t = 0.02$ and positions (from top to bottom) $Z = n\Xi_0$, $n = 1, 4$.

change field parameter I is weak, of the order of Δ_0/E_{FS} . Possible resonance effects have been predicted to occur at these small exchange energies.⁴³ Results are shown in the right column of Fig. 8. For the values of the parameters considered in this subsection, it follows from Table I and the BCS relation $k_F\xi_0 = (2E_F)/(\pi\Delta_0)$ that $\Delta_0/E_{FS} = 0.0127$ here. We consider the same temperature and location in the superconductor as for the larger values of I in the left column of the Figure. We start with the case $I = \Delta_0/E_{FM}$, (top curve in this column). Focusing on energies $|\epsilon/\Delta_0| < 1$, we see a dramatic sharp peak in the DOS near the gap edge, and five smaller peaks at lower energies. Upon doubling I , (second panel from top) the sharp peak structure near $\epsilon/\Delta_0 = 1$ vanishes, and there are now four subgap small peaks. Indeed, we have found that the sharp peak exists only at $I = \Delta_0/E_{FM}$. Finally, the bottom curve shows that for $I = 3\Delta_0/E_{FM}$, only three small subgap peaks remain. It would be of considerable interest to verify experimentally the appearance and disappearance of the very sharp peak at the gap edge for $I = \Delta_0/E_{FM}$.

Examination of the bottom (superconductor side) panels of Figs. 1, 2, 3 and 4, shows that the exchange

field seems to affect the pair amplitude $F(Z)$ within the superconductor relatively little over any significant length scales. We want to study the possibility, however, that the differential local DOS $\delta N(\epsilon, z)$, defined in Eqn. (11) may show, within the superconductor, magnetic penetration over distances much larger than that revealed by $\Delta(z)$. We have a hint that this might be the case: the results for $\Delta(z)$ in Ref. 34, exhibited no significant dependence on I , while $\delta N(\epsilon, z)$ was appreciably nonzero within a small region in the superconductor near the interface. These previous results were obtained for the special case where $k_{FS} = k_{F\uparrow}$, a condition, which corresponds to an I dependent mismatch parameter $\Lambda = 1/(1+I)$, that may yield results different from the case $\Lambda = 1$ considered here.

We examine in Fig. 9, the normalized $\delta N(Z)$ for a field parameter values $I = 1/4$ (left column) and $I = 1$ (right column). We use $t = 0.02$ and choose four locations in the superconductor, at $Z = n\Xi_0$, $n = 1, 4$. At the position $Z = \Xi_0$, (top panels) there is a clear manifestation of the magnetic proximity effect through a nonzero value of δN near $\epsilon/\Delta_0 = 1$. The effect decreases as Z increases and, for $I = 1/4$ it nearly dies out at $Z = 4\Xi_0$, that is, after several coherence lengths. At $I = 1$ (half metallic case) the effect is more prominent and extends over larger distances. However, the integral of δN over energies turns out to be always extremely small (as we shall see below) at these distances, at which only the self consistent energy spectral distribution shows magnetic penetration spin-splitting effects. We see that δN vanishes at the Fermi level but the details of this fairly long range redistribution of energy states are nontrivial and difficult to interpret. Nevertheless, that the effect is larger near the gap energy can be readily understood if one recalls that⁴⁴ the imaginary part of the wave vector of injected quasiparticles below the gap (in a non-self consistent approach) vanishes as the gap edge is approached.

In previous work³⁴ it was found as mentioned above, that for $I = 1$ and no mismatch between the spin up and superconductor band ($E_{F\uparrow}/E_{FS} = 1$), the effect of the exchange field on the superconductor was small and $\delta N(Z)$ decayed away over a few atomic distances. However the current condition $\Lambda = 1$ implies, at $I = 1/4$ and particularly at $I = 1$ a considerable mismatch between k_{FS} and $k_{F\uparrow}$. We shall study this point in detail below, in the context of our discussion of wave vector mismatch in general.

2. Fermi wavevector mismatch

In the last paragraph, we have seen that, (as previously³⁰ seen in a different context) mismatch among the three Fermi wave vectors involved in the problem (or the three band widths) may have a considerable effect on the results. As such mismatch is experimentally unavoidable, we now proceed to investigate it in some detail.

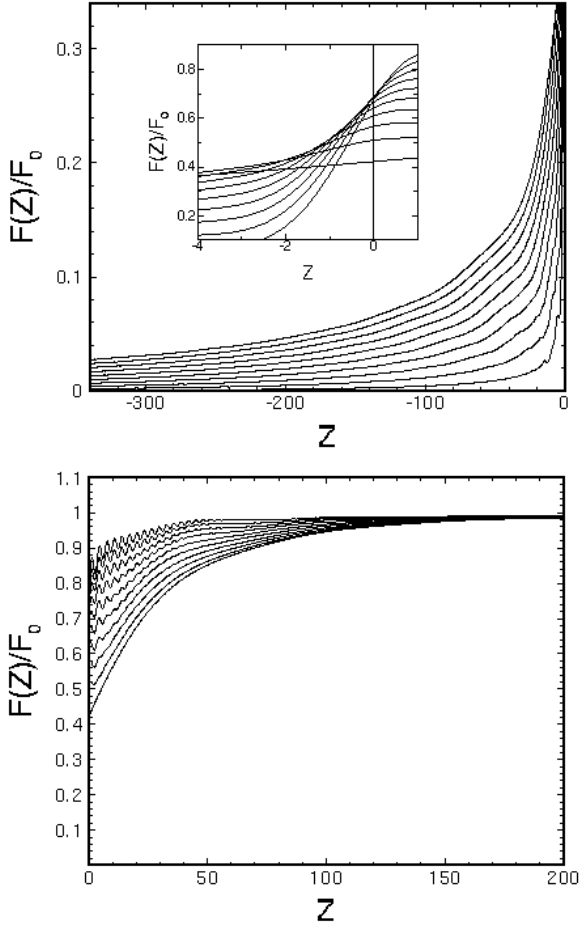


FIG. 10. $F(Z)$ at $t = 0.1$ and $I = 0$, plotted vs. Z , for values of the mismatch parameter Λ (see Table I) $\Lambda = 0.1 - 1$, in increments of $1/10$. Top panel is the normal metal region: the curves, from top to bottom, correspond to decreasing Λ . The bottom panel is for the superconductor, and curves from top to bottom correspond to increasing Λ . Inset: crossing of the curves close to the interface (vertical line) on the normal side emphasizing that $F(Z)$ is continuous.

Thus, we will consider values of the mismatch parameter Λ (Table I) different from unity. We will still keep the interface barrier parameter at $H_B = 0$.

In Fig. 10 we show the pair amplitude for $I = 0$, $t = 0.1$, and Λ varying from the previous case of unity down to 0.1 in increments of $1/10$. We focus on the situation where the bandwidth in the normal metal is smaller than that of the superconductor. This is the more common situation in F/S structures and in any case, it turns out to lead to more prominent effects. The top panel in Fig. 10 shows an overall suppression of superconducting correlations with decreasing Λ (increasing mismatch). Extremely near the interface, $|Z| \approx 1$, (see inset), $F(Z)$ drops rapidly and the curves cross as Λ increases. At $\Lambda = 0.1$ (bottom curve in this main panel) the phase coherence is virtually destroyed at the the distance of $Z = -200$. Away from the interface, the pair correla-

tions still decay in accordance with Eqn. (12), the only modification being a mismatch dependent amplitude factor $g(\Lambda)$,

$$F(Z) = \frac{g(\Lambda)}{|Z| + c_2}, \quad (21)$$

where $g(\Lambda)$ is an increasing function of Λ . Thus, a smaller bandwidth in the normal metal tends to restrict the influx of Cooper pairs. Physically, since the parallel momentum of a Cooper pair at interface is conserved, the longitudinal component is restricted by the smaller number of states accessible in the normal side.²⁹ This is consistent with the bottom panel of Fig. 10 which shows $F(Z)$ in the superconductor. The top curve, corresponding now to $\Lambda = 0.1$, shows a smaller characteristic length of decay from the interface than that for the $\Lambda = 1$ case (bottom curve). The subsequent value of $\Delta(Z)$ at the interface, Δ_{MIN} , decreases smoothly as Λ increases. The effects of values of Λ in the range $\Lambda > 1$, (not shown) are in the opposite direction, but always much less prominent. For this reason this range has been deemphasized.

The general trends are similar in the ferromagnetic case. The top panel of Fig. 11 displays the damped oscillations of $F(Z)$ in the magnet, at $I = 1/2$. The period of the damped oscillations varies inversely with $\sqrt{\Lambda}$, in agreement with Eqn. (18), but they nearly wash out when $\Lambda = 0.1$. Also, the sharp monotonic decline very near the interface increases in slope with greater Λ , so that $F(Z)$ first reaches zero at a greater distance from $Z = 0$, thus also increasing $k_{FS}\xi_1$ defined earlier. Quantitatively, one can obtain an excellent fit for the damped sinusoidal dependence of the pair amplitude by using Eqn. (20) with $k_{FS}\xi_2$ as a fitting parameter. The results of doing this yield values in excellent agreement with Eqn. (18).

In the bottom panel of Fig. 11, the top five curves show the drop in $F(Z)$ within the superconductor as the interface is approached. The main feature that stands out is that the results in the range $0.7 < \Lambda < 1$ are nearly independent of Λ , while those for $\Lambda < 0.7$ exhibit a marked Λ dependence, similar to that seen in the bottom panel of Fig. 10. This unexpected result arises as at $I = 1/2$ and $\Lambda = 2/3$ one reaches the special point where $E_{F\uparrow} = E_{FS}$. This property is further exemplified in the inset where we present Δ_{MIN} as a function of Λ . One can see a kink in the curve at about $\Lambda = 2/3$.

The Fermi wavevector mismatch influences also the local DOS as shown in the following figures. Starting again with $I = 0$, we present in Fig. 12 the normalized DOS in (left column) the normal metal at $Z = -100$ for three different values of $\Lambda \neq 1$, and (right column) for the superconductor at $Z = 1\Xi_0$, at the same Λ values. The corresponding $\Lambda = 1$ results are in Fig. 6. Both cases are at the low temperature of $t = 0.02$. As Λ decreases, (higher mismatch) we see that, for $\epsilon/\Delta_0 < 1$, the bound state peaks decrease, until they disappear at $\Lambda = 0.1$. The decrease at higher energies reflects our normalization. The superconductor side (right column) shows an

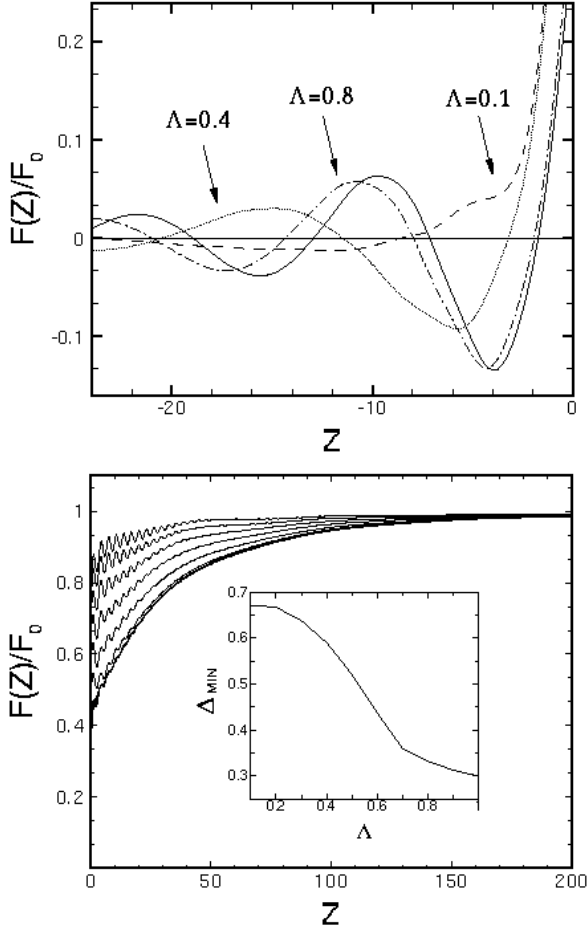


FIG. 11. Normalized pair amplitude for the case $I = 1/2$ and $t = 0.1$. The top panel illustrates the variation of $F(Z)$ for three different Λ (as indicated) in the ferromagnet, while in the superconductor side (bottom panel) results for the same Λ values used in Fig.10 are shown (in order of decreasing Λ from top to bottom). The inset depicts the value of $\Delta(Z)$ at the interface, Δ_{MIN} as a function of the parameter Λ

interesting trend. We examine there the point $Z = 50$, one coherence length away from the interface. As one decreases Λ , the small but distinct peaks within the gap turn into small wiggles at $\Lambda = 0.4$ and disappear altogether for $\Lambda = 0.1$. The BCS peaks at the gap edge become much more pronounced, indicating a substantial reduction in Andreev reflection at the interface because of the increased mismatch in Fermi energies, which results in superconductivity being more “confined” to the superconductor.

We saw in Fig. 11 that the damped oscillations of the pair amplitude inside the magnet increase in wavelength and decay quicker with decreasing Λ (increasing mismatch). We investigate the effect this has on the DOS in Fig. 13 for the same value of I , $I = 1/2$, as in that Figure. The left column of Fig. 13 depicts the changes in the magnet side local DOS associated with the same variation in Λ presented for $I = 0$ in Fig. 12. Corresponding

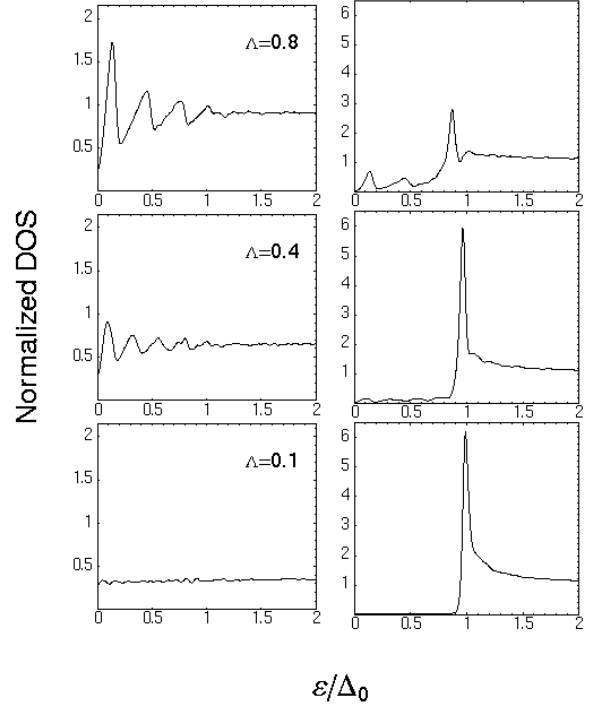


FIG. 12. Normalized local DOS plotted versus the dimensionless energy ϵ/Δ_0 at $I = 0$, and $t = 0.02$ for three values of the mismatch parameter Λ labeled in the left panels. The position is at $Z = -2 \Xi_0$ in the normal metal side (left column), and at $Z = \Xi_0$ in the superconductor side (right column).

results at $\Lambda = 1$ were given in Fig. 7. As expected the DOS again experiences oscillations correlated with the characteristic length $k_{FS}\xi_2$, as a function of Λ . The left arrangement of panels in Fig. 13 illustrates this point. The coordinate is fixed to $Z = -4$. One can see an evident inversion between the $\Lambda = 0.8$ and $\Lambda = 1$ (Fig. 13) cases, whereby the positions of minima and maxima are interchanged. The superconductor side is examined in the right column, which shows the same Λ values as in the left set of panels, at a distance Z of one correlation length inside the material. The top panel exhibits behavior similar to that found for $\Lambda = 1$: the density of states within the gap is appreciably nonvanishing, and the peaks at $\epsilon/\Delta_0 = 1$ are relatively low. The peaks near the gap edge for $\Lambda = 0.4$, below are more prominent and there is a concomitant decrease in subgap states. This is quantitatively different from what we saw at $I = 0$, where there were more subgap states and the BCS peaks were significantly sharper. Finally, the bottom panel reveals a near absence of states below the gap, and the usual BCS-like peaks at $\epsilon/\Delta_0 = 1$.

It was also seen in Fig. 11 that $F(Z)$ in the superconductor decayed away from its bulk value near the interface in a strongly Λ -dependent manner. To address whether this parameter also affects the spin-splitting in the superconductor, we now calculate $\delta N(z, \epsilon)$ defined in Eqn. (11). Figure 14 shows δN (still at $t = 0.02$ and nor-

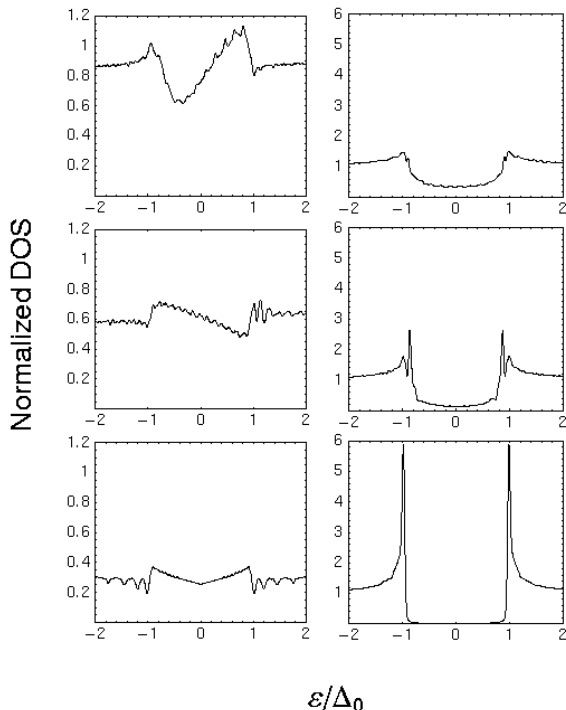


FIG. 13. Normalized local DOS for $I = 1/2$, and with the same temperature and Λ values used in Fig.12. The left column corresponds to the position $Z = -4$ in the ferromagnet, while the right column corresponds to $Z = \Xi_0$ in the superconductor.

malized as in Fig. 9) as a function of the dimensionless energy and at a distance of one ξ_0 from the interface, for several values of Λ , at $I = 1/2$. Starting at $\Lambda = 1$, we see an effect reminiscent of what was seen in Fig. 9: there is a net negative spin population for $\epsilon/\Delta_0 \lesssim 0.85$, then for larger energies, a greater number of up spin states, which decays quickly so that the two spin states equalize for $\epsilon/\Delta_0 > 1.5$. Next, consider the case where $\Lambda = 2/3$ (when $k_{F\uparrow} = k_{FS}$). In agreement with Ref. 34 the result is nearly zero for this special value. This value of Λ is also the point at which the $F(Z)$ plots (Fig. 11) start diverging with further decreases in Λ . At this special matching point little leakage of magnetism into the superconductor occurs. The importance of this crossover point becomes more evident in the remaining curves, where the mismatch parameter is decreased to $\Lambda = 0.4$ and then to 0.1. The sign of the δN variations with energy is reversed. This pattern, and the relatively large maximum and minimum values of δN reflect that the high peaks reached by the DOS at these values of Λ (see Fig. 13, right column), occur at slightly different values for the up and down spin bands. Again, the magnetic moment at those distances is very small: if one integrates the normalized δN over the variable ϵ/Δ_0 the result is of order 10^{-2} at $Z = \Xi_0$, changing sign at $\Lambda = 2/3$. Only very near the interface, at values of Z of order unity, we find that this integral is larger, and of course always

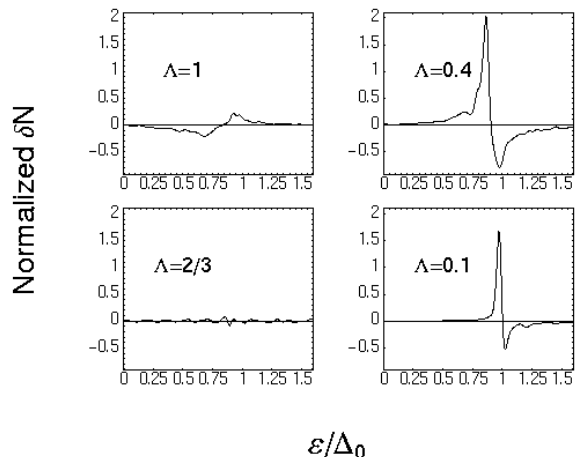


FIG. 14. Normalized δN [see Eq.11], at $Z = \Xi_0$ in the superconductor for different values of Λ .

positive. As a rule, spin-splitting effects in the self consistent DOS extend through several times ξ_0 (being larger near $\epsilon/\Delta_0 = 1$ for the reasons already discussed), except of course at the reversal point. The parameter characterizing the degree of wavevector mismatch is therefore important in the study of proximity effects on both sides of the F/S interface.

3. Interface scattering

Up to this point we have considered only transparent interfaces. A thin oxide layer at the interface adjoining a superconductor and a normal metal or ferromagnet can be modeled by a repulsive delta function potential as defined earlier in Sec. II. The spin independent scattering strength is parameterized in dimensionless units by the quantity H_B , defined in Table.I.

We fix the temperature to $t = 0.1$ and the mismatch parameter to unity for this study. In Fig. 15 we present the pair amplitude in both the superconductor and the normal ($I = 0$) metal, in the format of previous Figures. We consider five equally spaced values of the dimensionless barrier strength ranging from $H_B = 0$ to a relatively strong interfacial scattering barrier $H_B = 0.8$. First we examine the normal metal side, in the top panel. The effect of the barrier is quite pronounced, as the pair amplitude still decays slowly into the normal side, but with an overall large decrease in amplitude. Also evident are Friedel type⁴⁵ oscillations in $F(Z)$ near the interface: as the insulating barrier becomes stronger, the two parts of the system become more isolated from each other. The pair amplitude in the region shown is adequately fit by the functional form of Eqn. 12 but with the parameters c_1 and c_2 being both functions of H_B . Within the superconductor, the pair correlations within a range of order ξ_0 from the surface increase with increasing barrier strength. This is illustrated in the bottom panel of

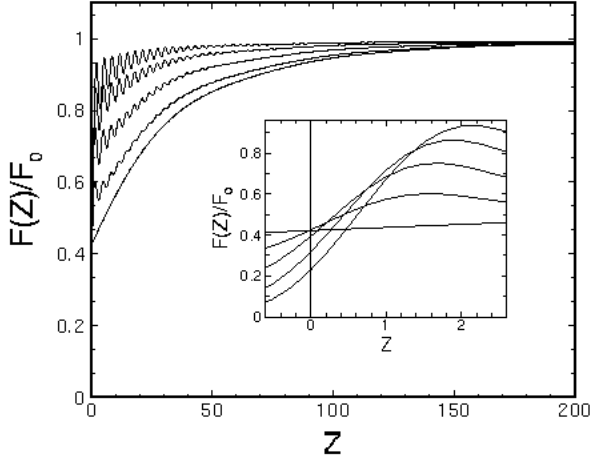
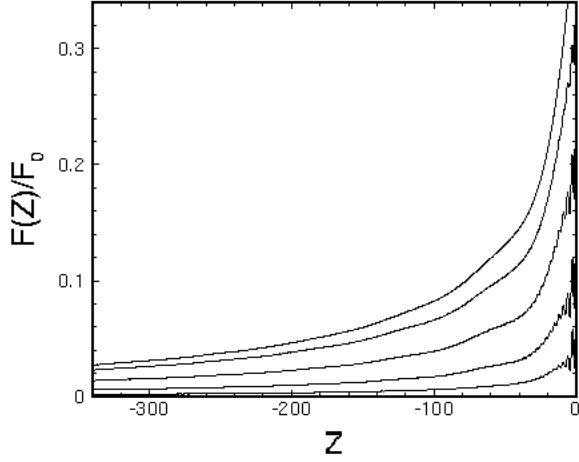


FIG. 15. The normalized pair amplitude at $I = 0$ for different values of the barrier strength (see Table I), $H_B = 0, 0.2, 0.4, 0.6, 0.8$, and $t = 0.02$. The top panel is for the normal metal region. The curves, from top to bottom, correspond to increasing H_B . The bottom panel depicts the superconductor side. The curves from top to bottom are in order of decreasing H_B in this region. The inset reveals the crossing of the curves near the interface (vertical line) at length scales too small to be seen in the main panel.

Fig. 15, where the rise of $F(Z)$ near the interface can be seen to sharpen with increasing H_B . The top curve ($H_B = 0.8$) has the least overall variation in the scale shown. The oscillations near the interface have the same period as in the normal metal, and their amplitude increases with H_B . As remarked in connection with Fig. 10, $F(Z)$ is continuous at the interface, but here however, the curves cross in the superconductor very near the interface. This is illustrated in the inset since this property is not visible in the horizontal scale of the main figure, where we emphasize longer-range changes.

The case of a finite exchange field (with $I = 1/2$) is shown in Fig. 16. All other parameter values are the same as in Fig. 15. Examining first the magnet side, (top panel) reveals that the amplitude of the damped oscillations decreases as the scattering potential is increased.

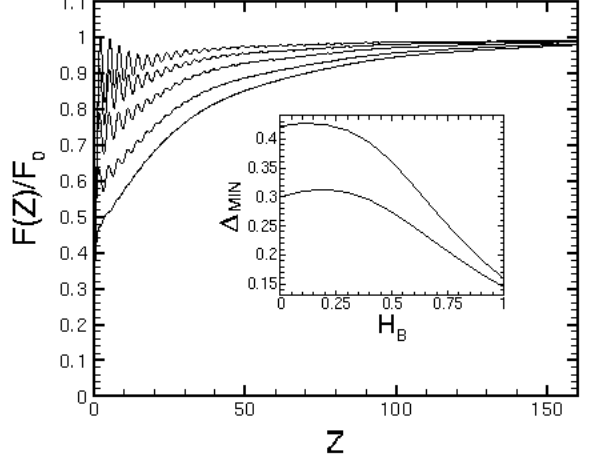
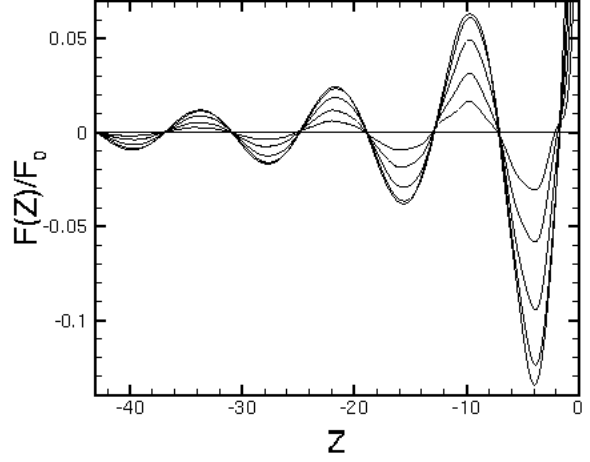


FIG. 16. Normalized pair amplitude at $I = 1/2$, for the ferromagnet (top panel), and the superconductor (bottom panel). All other parameters and curve trends are the same as in Fig.15. The inset illustrates the variation of Δ_{MIN} as a function of the barrier strength H_B .

The period is independent of H_B , in agreement with Eqn. (18). The additional decay of the amplitude of the oscillations can be incorporated into Eqn. (20) through a multiplicative factor that decreases linearly with H_B . The location of the first node of $F(Z)$ in the magnet is nearly unaffected, demonstrating that both the characteristic length scales $k_{FS\xi_1}$ and $k_{FS\xi_2}$ are independent of interface transparency. On the superconductor side, the bottom panel shows how the length scale over which $F(Z)$ regains its bulk value from the interface decreases as the scattering potential increases. We again see oscillations in $F(Z)$ for finite values of H_B , near the interface, here they are more marked than in the $I = 0$ case. The value of Δ_{MIN} at a given H_B always decreases with I . This is illustrated in the inset at the bottom of Fig. 16, where we plot Δ_{MIN} as a function of H_B , for two values of I . The difference between the two curves is largest at $H_B = 0$, while they trend closer with increasing barrier strength. As the barrier becomes very strong the

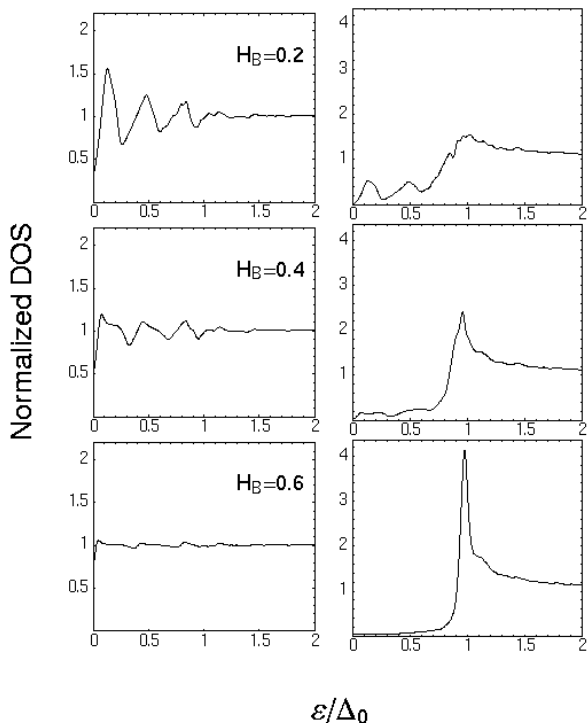


FIG. 17. The effect of a finite barrier on the local DOS: Normalized local DOS at $I = 0$ for finite values of the barrier strength $H_B = 0.2, 0.4, 0.6$ and temperature $t = 0.02$. The left column corresponds to $Z = -100$ in the normal metal, and the right column is for $Z = \Xi_0$. The value of H_B at each panel on the right is the same as that in the panel on its left.

proximity effects become minimal.

We conclude this subsection with a look at how the local DOS is modified due by finite barrier strength. In Fig. 17, we display the normalized local DOS for $I = 0$, at $t = 0.02$. The left column shows the results for the normal metal side. The curves all correspond to $Z = -100$. The $H_B = 0$ results are in Fig. 6, while here we show results for increasing values of H_B as labeled in the figure. The general trend on increasing the scattering potential is a reduction in the magnitude of the peaks for subgap energies. The characteristic energy spacing E_c shows relatively little change, but the shape of the peaks is drastically altered. The corresponding change in the DOS profile for the superconductor is shown in the right column, where we present the local DOS for the same values of the barrier strength and at the point $Z = \Xi_0$. The de Gennes St. James bound states still evident in the top curve become smeared out until at the bottom curve, where $H_B = 0.6$, the influence of the normal metal becomes almost nonexistent. Thus we find that although both the insulating barrier and the Fermi energy mismatch tend to destroy superconducting order in the non-superconductor, their DOS signature is quantitatively different.

The effect of barrier strength at finite exchange fields can be seen in Fig. 18. We take $I = 1/2$, with all other

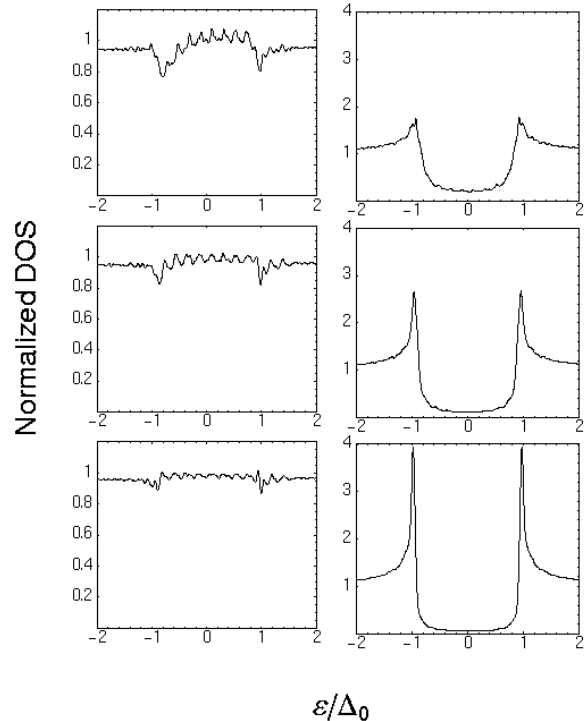


FIG. 18. Local normalized DOS for $I = 1/2$ and the same barrier strengths and parameter values used in Fig.17. The distance on the left side, however, is $Z = -4$ (left column) while on the superconducting side (right column) we have still $Z = 50$.

parameter values at the same values as in Fig. 17. In the ferromagnet side, the top left curve in Fig. 18 demonstrates a wide structure in the subgap DOS. Upon increasing the barrier strength (lower panels), there is a dramatic reduction in this structure. As can be seen, when the barrier strength is rather large ($H_B = 0.6$), the DOS shows very minimal signs of the proximity effect at the distance from the interface considered. The superconductor side (right column), for $Z = \Xi_0$ and the same values of H_B as the other panel, reflects the trend seen in the ferromagnet. The subgap states at zero barrier (top curve, see also Fig. 8) gradually disappear with increasing H_B , while simultaneously sharp BCS peaks develop. For $H_B \geq 0.5$, the results follow closely the $I = 0$ case (see Fig. 17(b)) since the influence of the non-superconductor material has vanished. These results illustrate the importance of fabricating samples with good, clean interfaces.

B. Structures

All of the above results pertained to “bulk” structures, in that both slabs were taken to have dimensions significantly larger than the zero temperature BCS coherence length. We now address what happens when either the ferromagnet or the normal metal is thin enough so that size effects are appreciable. A bilayer system of this type

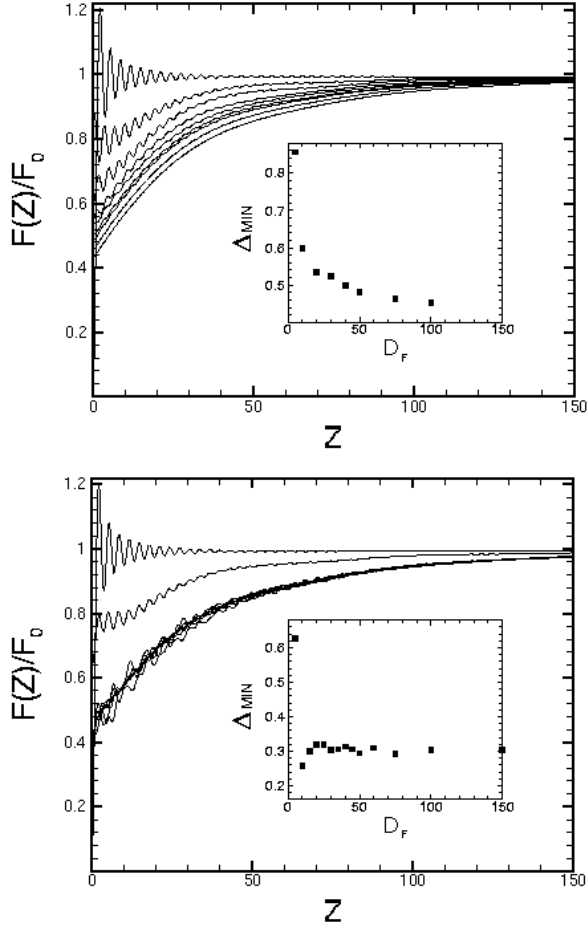


FIG. 19. Pair amplitude in a superconductor in proximity to a non-superconducting layer of finite thickness D_F (see text). The top panel shows results for $I = 0$. The curves from top to bottom correspond to $D_F = 0, 5, 10, 20, 30, 40, 50, 100, 200$, respectively. The bottom panel has results for $I = 1/2$. The top two curves are for $D_F = 0, 5$. The other curves, all of which essentially coincide, are for the remaining values of D_F as shown in the top panel. The insets show Δ_{MIN} vs D_F in each case.

is an appropriate model for the case when the mean free path in the finite layer is larger than the layer's width. We will present a broad range of results, varying D_F from a few atomic spacings up to of order Ξ_0 , while keeping $D_S \gg \Xi_0$, and vice versa. We will consider the case where both D_F and D_S are small in Sec.III C. For the sake of brevity, we will take the interface to be transparent ($H_B = 0$), the mismatch parameter to be $\Lambda = 1$, and fix the temperature to $t = 0.02$.

We begin with a normal metal ($I = 0$) of finite width backed by a “bulk” superconductor, taken here to be $D_S = 16\Xi_0$. The top panel in Fig. 19 shows the pair amplitude in the superconductor for various normal metal widths. We show $F(Z)$ only for the superconductor side since the pair amplitude in the finite normal side is cut off at different distances. The top curve corresponds to

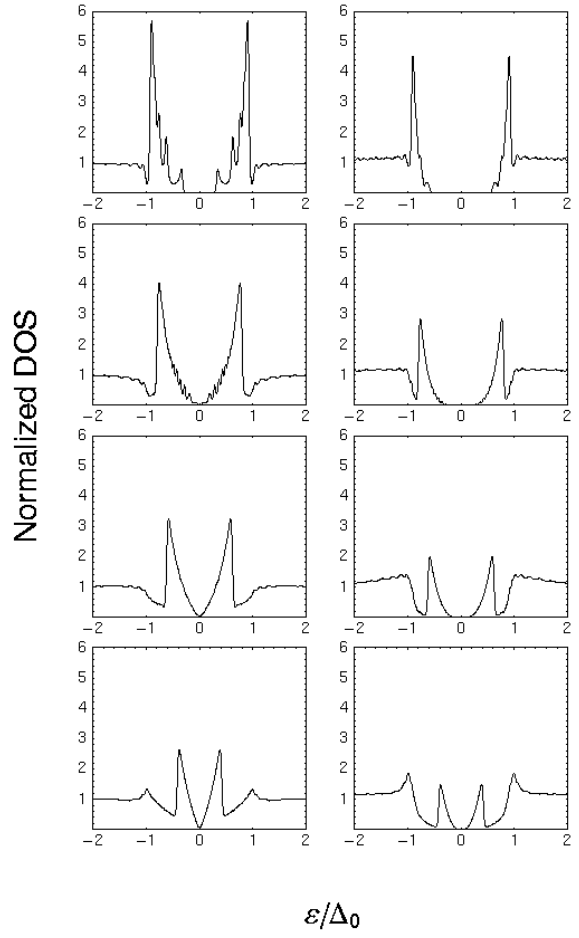


FIG. 20. Local DOS for the same geometry analyzed in Fig. 19, at $I = 0$. From top to bottom, each set of panels corresponds to $D_F = 20, 50, 100, 200$. The left column shows the normal metal ($I = 0$) local DOS $N(z, \epsilon)$, spatially averaged over one Ξ_0 as described in the text. The right column is the local DOS at $Z = 50$ in the superconductor.

a single superconductor slab (zero width for the normal metal), while subsequent curves are for increasing normal metal widths ranging up to $D_F = 200$. The oscillations near the interface at zero or very small D_F , are again the well-known geometrical Friedel oscillations. The largest changes in the pair amplitude near the interface occur for $0 < D_F < 20$. When $D_F \geq 50$, the characteristic length scale for superconducting depletion is given approximately by the coherence length ξ_0 . The inset displays Δ_{MIN} (as usual, the value of $\Delta(Z = 0)$) as a function of D_F . It is seen that Δ_{MIN} drops rapidly until about $D_F = 50 = \Xi_0$ and thereafter it decays more slowly.

The same geometry as in the top panel of Fig. 19 but with the finite non-superconducting layer being ferromagnetic ($I = 1/2$) is considered in the bottom panel of this Figure, which again depicts the pair amplitude in the superconductor. As the ferromagnet thickness D_F begins to increase from zero the pair amplitude drops

very rapidly, as in the $I = 0$ limit. A notable distinction exists here however. When D_F is larger than about $D_F = 10$, the characteristic length scale over which $F(Z)$ rises to its bulk value becomes approximately independent of D_F . This behavior is also seen in more detail in the inset of the same Figure where we plot Δ_{MIN} as a function of D_F . The decay of Δ_{MIN} occurs nearly entirely in the region $D_F \leq 10$, while for $I = 0$ it takes place over a much more extended range. This of course reflects that the superconducting penetration (at low T) into the normal metal is very large, while for a magnet with $I = 1/2$ it is characterized by a length of order ξ_2 . Once D_F reaches that limit, further increases are ineffective.

We have also calculated the DOS for the geometries used in Fig. 19. Since the non-superconductor layer is in some cases quite thin ($D_F < \Xi_0$), the local DOS in the normal region exhibits strong oscillations as a function of Z . For this reason, we present results for the spatial average of $N(Z, \epsilon)$ over a distance in the Z direction equal to the layer thickness D_F if $D_F < \Xi_0$, or over one dimensionless coherence length, Ξ_0 , if $D_F > \Xi_0$. In the latter case this average is centered at $Z = -D_F + \Xi_0/2$. We present in the left column of Fig. 20, the averaged DOS within the normal ($I = 0$) metal for four different thicknesses, at $t = 0.02$. The top left panel corresponds to a thin film with $D_F = 20$ (recall the superconductor is in the bulk limit). A clear “mini gap” structure is present. As D_F is increased to $D_F = 50$, a much smaller gap remains, and multiple ripples rise to two larger bound state peaks. If D_F is doubled again to $D_F = 100$, the gap disappears. Upon increasing D_F further to $D_F = 200$, we see another peak emerge and form the initial stages of the sawtooth-like profile seen earlier in bulk systems (see Fig. 6). Thus we find that there exists a maximum thickness for the normal metal $D_F \approx \Xi_0$, such that, if exceeded, the gap in the normal side DOS disappears. The observed filling in of the states originates from quasiparticles with relatively large momenta parallel to the interface ($k_{\perp} \approx k_{FS}$).

In the right column of Fig. 20, the local DOS in the superconductor at a distance $Z = \Xi_0$ from the interface is shown. Here we do not spatially average the local DOS, since we are in the bulk regime and the DOS varies smoothly. We present the local DOS at $Z = \Xi_0$, while all other parameters take the values used previously in the left column. The top curve ($D_F = 20$) shows a widening of the gap, while the main peaks still remain below $\epsilon/\Delta_0 = 1$. The panel below demonstrates the bound state peaks being pushed further towards the Fermi level. For $D_F = 100$, the single pair of peaks has moved inward even further as a marked through develops at $\epsilon/\Delta_0 \approx 1$. The effect is more pronounced in the bottom curve, where $D_F = 4\Xi_0$, and the de Gennes St. James states have become smaller than the main peaks that have formed near the gap edge, which eventually develop into BCS-like peaks deeper within the superconductor.

We consider next the DOS when the non supercon-

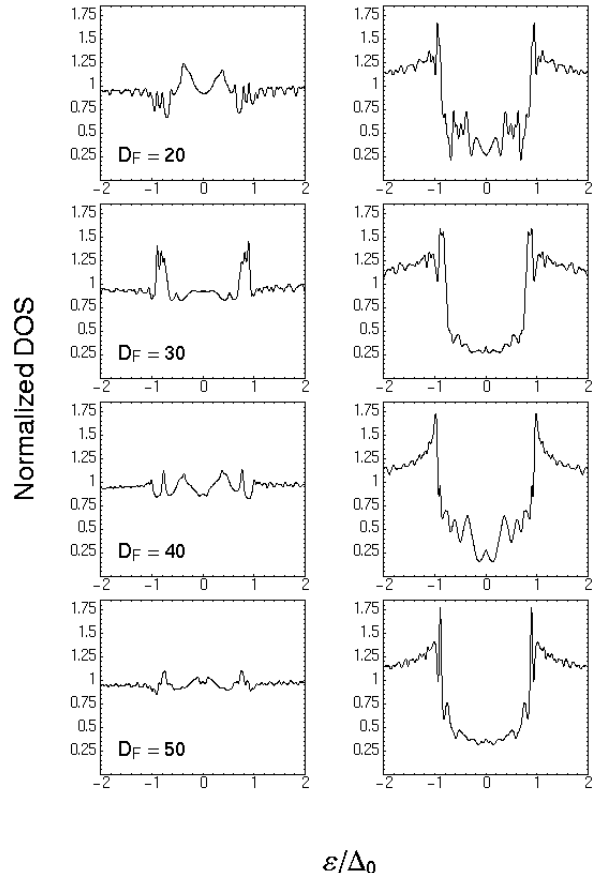


FIG. 21. Local DOS as in the previous Figure, but for $I = 1/2$. From top to bottom each pair of panels corresponds to $D_F = 20, 30, 40, 50$.

ductor layer in the system is a ferromagnet. We present results at $t = 0.02$, and $I = 1/2$, as in the bottom panel of Fig. 19. In the magnetic side, we spatially average the DOS over its width D_F as described above. The result is shown in the left column of Fig. 21. The top curve exhibits two slightly asymmetric peaks at $\epsilon/\Delta_0 \approx 0.2$. The structure seen there is washed out at larger D_F . There is no gap in the ferromagnet DOS shown but we found⁴² a mini-gap when D_F is small ($D_F \approx k_{FS}\xi_2$). The local DOS at the point $Z = \Xi_0$ inside the superconductor is illustrated in the right column of Fig. 21. In the top curve ($D_F = 20$), it is seen that the highermost peaks are shifted slightly towards lower energies ($\epsilon/\Delta_0 \approx 0.9$) compared with the bulk BCS result. At even lower energies there is a relatively high number of subgap states. Upon increasing the ferromagnet’s width to $D_F = 30$, the coarse structure seen previously becomes somewhat smoothed out. On the curve below ($D_F = 40$), numerous peaks have returned within the gap, and then diminish again in the the last curve for $D_F = 50$. We find therefore that the presence of the magnet next to the superconductor results in more prominent features in the DOS, at smaller D_F values.

We now reverse the role of the two materials in the

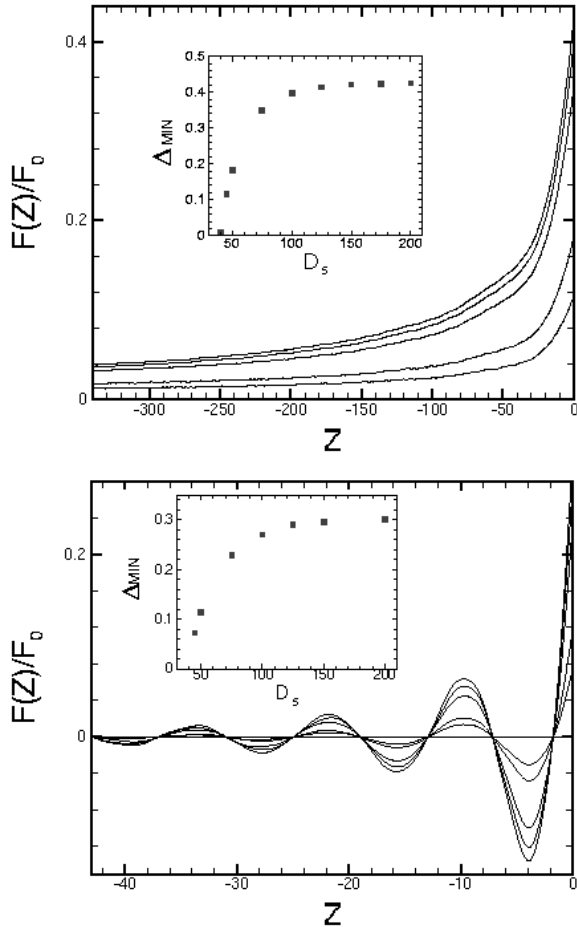


FIG. 22. Pair amplitude for a structure consisting of a superconductor of finite thickness D_S adjoining a thick non-superconductor. The main plot in the top panel shows the decay of the pair amplitude in the normal metal ($I = 0$) for values of $D_S = 200, 100, 75, 50, 45$. The bottom panel shows the pair amplitude at $I = 1/2$ and the same geometry. The values of D_S are the same as in the top panel, and the amplitude of the oscillations decays with decreasing D_S . The insets illustrate the behavior of Δ_{MIN} vs D_S in each case.

bilayer, that is, we consider a very thick “bulk” ferromagnet (we take $D_F = 16\Xi_0$ as was done above for D_S), in contact with a finite superconductor layer. Temperature and other parameters are as in the previous case. In order to study fully the geometrical effects associated with varying the superconductor thickness, we shall consider a wide range of widths D_S , taking Ξ_0 close to the lower bound, since the superconductor ceases to maintain pairing correlations when $D_S \lesssim \Xi_0$.

The top panel of Fig. 22 shows the modification of the pair correlations in a bulk normal metal ($I = 0$) that occur as the width of the superconductor varies. The top curve ($D_S = 4\Xi_0$) differs relatively little from the situation where both the normal metal and superconductor were in the bulk (compare with Fig. 1). A decreasing trend is followed as D_S decreases. The slow

decay of $F(Z)$ away from the interface is adequately fit by Eqn. (20) for $D_S \geq 1.5\Xi_0$, the only modification being an overall D_S -dependent factor that reduces the amplitude. The bottom two curves, corresponding to $D_S = 0.9\Xi_0, \Xi_0$ have an even slower decay. The inset depicts the corresponding change in the pair potential at the interface, Δ_{MIN} , as a function of D_S . This inset emphasizes the fast rise in the pairing correlations at the interface when D_S is on the scale of Ξ_0 , and it includes additional values of D_S not presented in the main figure.

In Fig. 22 (bottom panel) we show the damped oscillations of $F(Z)$ within the ferromagnet ($I = 1/2$) for the same values of D_S as in the top panel. The main effect of changing D_S is to reduce the amplitude of the oscillations while their period remains, as expected, the same. Their amplitude however, drops very markedly when D_S approaches Ξ_0 . This is illustrated in the inset, where we display Δ_{MIN} versus D_S . The essential behavior is similar to that in the $I = 0$ case in the other panel, whereby Δ_{MIN} changes the most for $D_S < 1.5\Xi_0$. The overall magnitude is reduced, however, by the finite value of the exchange energy.

The local DOS is also sensitive to the spatial extent of the superconductor. The left column in Fig. 23 shows the normalized local DOS at $Z = -100$ in the $I = 0$ limit, for several values of D_S . Spatial averaging in this case is unnecessary. For $D_S = 200$ (top curve), it is evident that this width is sufficient for Andreev reflection to become well established, and hence for the complete formation of the structure seen in the bulk case (see Fig. 6). At $D_S = 2\Xi_0$, even though D_S is still larger than Ξ_0 , the DOS profile has changed its shape so that the peaks slant in the opposite direction. The magnitude of the peaks has decreased slightly overall, but their characteristic energy spacing E_c remains the same with the exception that the largest peak has slightly shifted towards smaller energies. The next curve ($D_S = 1.5\Xi_0$) shows how this trend extends further. Finally, when $D_S = \Xi_0$, only a slight hint of structure remains. These results reflect that the de Gennes St. James peaks arise mainly from Andreev reflection at the normal metal superconductor interface, so that when D_S decreases, so does the minimum gap (see Fig. 22 inset in the top panel). Next, we examine the DOS in the superconducting side (right column), using the same parameters as for the left side panels. We perform a spatial average over one coherence length centered around $Z = D_S - \Xi_0/2$ (in analogy with the thin magnet case). Beginning with the top curve and proceeding downwards, we see a rapid filling in of subgap states. As D_S is decreased (lower curves), any remnant of subgap states becomes smeared out due to the greater influence of the normal metal on the superconductor for smaller D_S .

We conclude this subsection by considering a finite exchange energy of $I = 1/2$ in the ferromagnet, with all other material parameters being identical to those in Fig. 23. As mentioned above, for a bulk superconductor juxtaposed to a bulk ferromagnet, the oscillatory pair

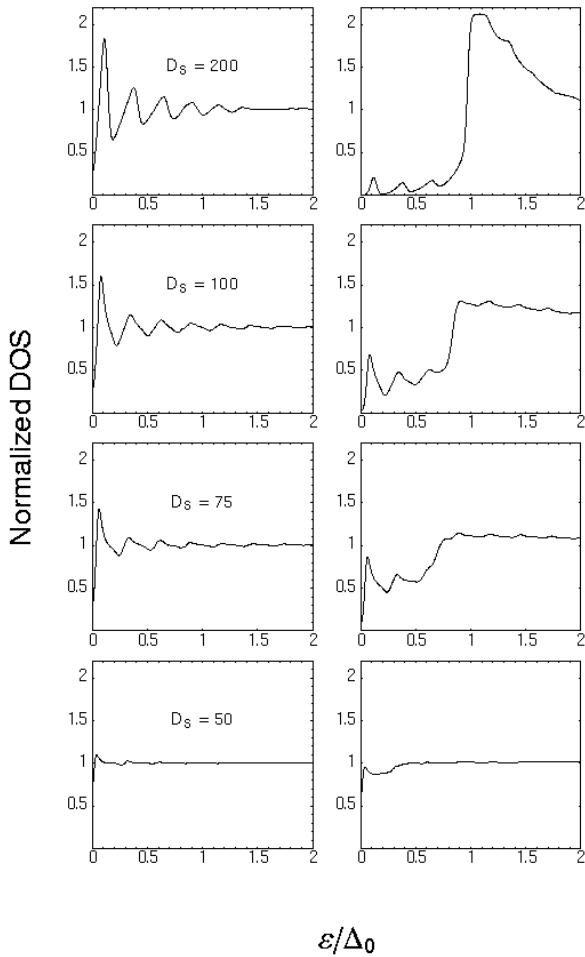


FIG. 23. Left column: localized DOS at $Z = -100$ for the structure considered in Fig. 22, at $I = 0$ and superconductor widths as indicated. Right column: local DOS for the same structure, averaged over one Ξ_0 (see text) from the end of the superconductor, for the same D_S as in the left column.

amplitude in the ferromagnet induces oscillations in the DOS as a function of position within the ferromagnet (see discussion of Fig. 7). Here, we wish to examine any modifications on this behavior that may arise from a finite D_S . To this purpose, we present in Fig. 24 (left column) the local DOS at the position $Z = -3$ for several values of D_S . The top curve, corresponding to $D_S = 4\Xi_0$, shows a DOS profile with two rounded peaks near the gap edge, while the minimum is at $\epsilon/\Delta_0 = 0$. This is fairly similar to what was seen at the same distance in Fig. 7. To understand the behavior of the DOS for smaller D_S , we recall the spatial dependence of the pair correlations in Fig. 22. There it was found that the oscillations in $F(Z)$ did not undergo a change in period as the superconductor width decreased. Rather, there was a smooth reduction in amplitude as D_S decreased. This suggests that changes in the DOS with decreasing D_S would behave similarly. The other curves in the left column of Fig. 24 agree with this reasoning: the effect of reduc-

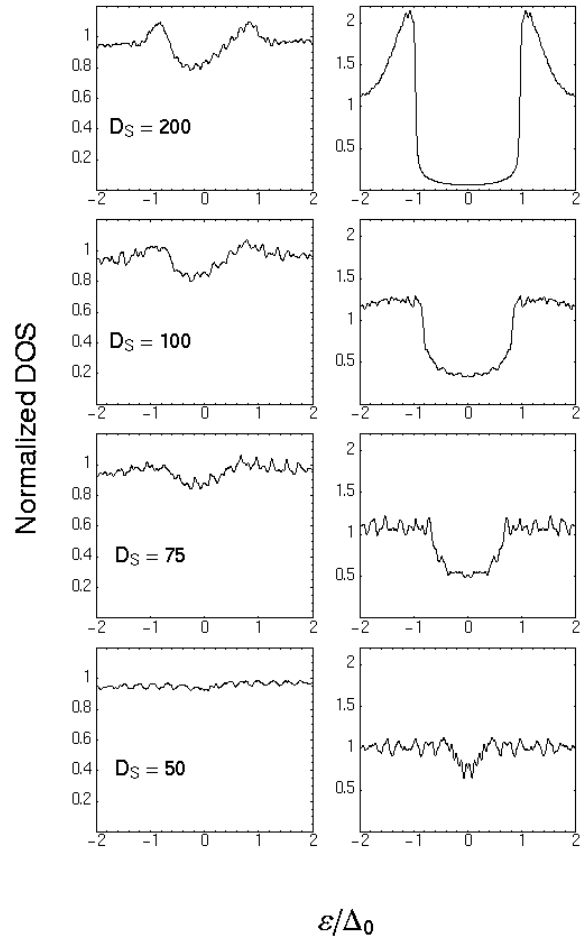


FIG. 24. Local DOS for the structure considered in Fig. 22 with $I = 1/2$. Left column: localized DOS at $Z = -3$ for $I = 1/2$ and superconductor widths as labeled. Right column: local DOS averaged over one Ξ_0 from the end of the superconductor for the same values of D_S as in the corresponding left column panels.

ing D_S is to lower peaks and raise minima, so that the leakage of superconducting order is effectively eliminated when $D_S = \Xi_0$.

The panels in the right column of Fig. 24 show the corresponding DOS in the superconductor, averaged over a distance of one Ξ_0 in the usual way. The top panel ($D_S = 4\Xi_0$, so that the average is taken centered at $Z = 175$) shows a clear but broad peak at $\epsilon/\Delta_0 \approx 1$, spreading over a significant energy range. This peak decays rapidly while shifting to smaller energies as D_S decreases. As D_S is reduced to $D_S = 2\Xi_0$, the states with energies $\epsilon/\Delta_0 \lesssim 1$ fill in rapidly while the primary peak is flattened. This trend continues until, at $D_S = \Xi_0$, there is hardly any evidence of the previous superconducting structure, indicating that superconductivity is nearly destroyed as the thickness is down to one correlation length.

C. Comparison with experiment

We have seen above that the calculated self-consistent results for the physical quantities depend in a systematic way on a number of parameters, some of which are related to the materials employed, while others are experimentally adjustable. While testing these systematic dependences is the task of future experimental work, we will, in this subsection, compare already existing experimental data with our theory. We will use data from direct local DOS measurements^{37,3} rather than results for indirectly derived quantities. Although we emphasize in this work the case where the non-superconductor is a ferromagnet, we will examine also the proximity effect when the normal metal is a ferromagnet. We will thus compare our calculations with the experimental data of Ref. 37 where DOS measurements were made from the normal metal side, and with data from Ref. 3, where local DOS measurements in the superconductor side of a magnet-superconductor structure were taken. In this way, we test our theory against spectroscopy data obtained by probing either side of the interface, in the two cases where the superconductor is in proximity to either a normal metal or a strong magnet. In making our comparisons, it is important to make pertinent choices for the applicable input parameters, as will be discussed below.

Consider first the STM data of Ref. 37, where the superconductor (Nb) is in contact with a non-magnetic metal (Au). The experimental configuration consisted of a thin layer of Au of thickness 200Å, that capped off a superconducting Nb dot. The Nb had a smooth relief resulting in a thickness (0 – 400Å) that decreased away from its center. We model this structure, as done in the experimental analysis³⁷, as a bilayer system comprised of a normal metal of constant width on a superconductor of varying thickness in the z -direction, in a manner similar to Sec. III B. We take $k_{FM} = 1\text{Å}^{-1}$, and we assume the normal metal to have a width of 200 Å. The transition temperature is $T_c = 9$ K. We assume the temperature to be $T = 270$ mK, a value which is slightly higher than the experimental value $T = 60$ mK. This is intended, in the usual way, to account for additional smearing effects associated with the finite energy resolution of the apparatus. The interfacial barrier strength parameter (H_B) is taken to be zero, which is appropriate for the clean, highly transparent interface used, and the Fermi wavevectors in the two materials are assumed to be equal. Other parameter values used in our calculations are the bulk Nb gap value $\Delta_0 = 2$ meV, which is close to the experimental value³⁷, and the Debye cutoff parameter $\omega = 0.03$, the value of this parameter having little effect on the results. The modeling of the superconductor width is less trivial since the Nb dot in fact varies in size not only in the z direction, but also in the transverse direction. With this in mind, we assume a superconductor thickness varying from 50 to 150 Angstroms. Because of possible nonuniformities in the composition of

the Nb dot, this quantity should be viewed as an effective thickness that accounts for any geometrical discrepancies between our model and the experimental configuration, and which may be interpreted to some extent as a fitting parameter. The final physical parameter needed is the coherence length ξ_0 . This parameter must be identified here as an effective correlation length to absorb the inherent effects of disorder in the system. Measurements were taken at several points: some, (which were labeled as points $a - d$ in Figure 1a of Ref. 37) were on the flatter part near the center of the dot. The others, labeled $e - j$ in that Figure, were in the sloping part near the edge. Disorder effects are likely to be more prevalent in the region in the latter points, where oxidation of the sample surface has a more pronounced effect on the superconducting order. Therefore we have set at $\xi_0 = 100\text{Å}$ in the region corresponding to the points $e - j$, while for in the region between the points $a - d$ we take $\xi_0 = 200\text{Å}$. These two sets of points were recognized as behaving differently in the original experimental analysis³⁷.

The geometry studied is not quite that in our earlier results of Sec. III B, where we varied the width of the superconductor in contact with an *infinite* normal metal. Here, both the normal metal and superconductor are effectively thin, and additionally, the assumed value of the coherence length is larger. Therefore, separate computations were required. We present in Fig. 25 the comparison of our results (solid line) to the the experimental data.³⁷ The DOS is scaled to its normal metal limit, with the curves shifted by a constant for illustrative purposes. The energy is in the same voltage units as in the experiment. Inspecting the spectra corresponding to the points $a - d$ (labeled in our Figure as they were in the experimental work), Fig. 25 demonstrates the excellent agreement between our results and the data. In the top panel, a BCS-like gap is most evident for the position the location labeled a , and as the effective superconductor width is decreased from 150 Å in a to 120 in d , the gap becomes smaller, while the BCS-peaks decrease in magnitude. The location of the peaks in the fits and in the experimental data are seen to essentially agree. A similar trend is seen for the remaining probe locations in the bottom panel of Fig. 25, where the effective coherence length and D_S are smaller. The peaks move inwards while the previously empty gap starts to fill in, with an approximately linear rise near the Fermi level. This DOS profile is observably different from that in the panel above, where the subgap DOS had a U-shape compared to the V-shape here. It is remarkable that the level of agreement between theory and experiment is so high, in that the location of the peaks as well as the origin of the minima in the DOS match well over the entire spatial range. Thus we find that modeling this particular experimental structure as a bilayer is successful over the entire spatial range. In Ref. 37 where it was found that a fit to all the data using the Usadel equations was not possible and that very different physical assumptions had to be used for the U- and V-shaped portions. This

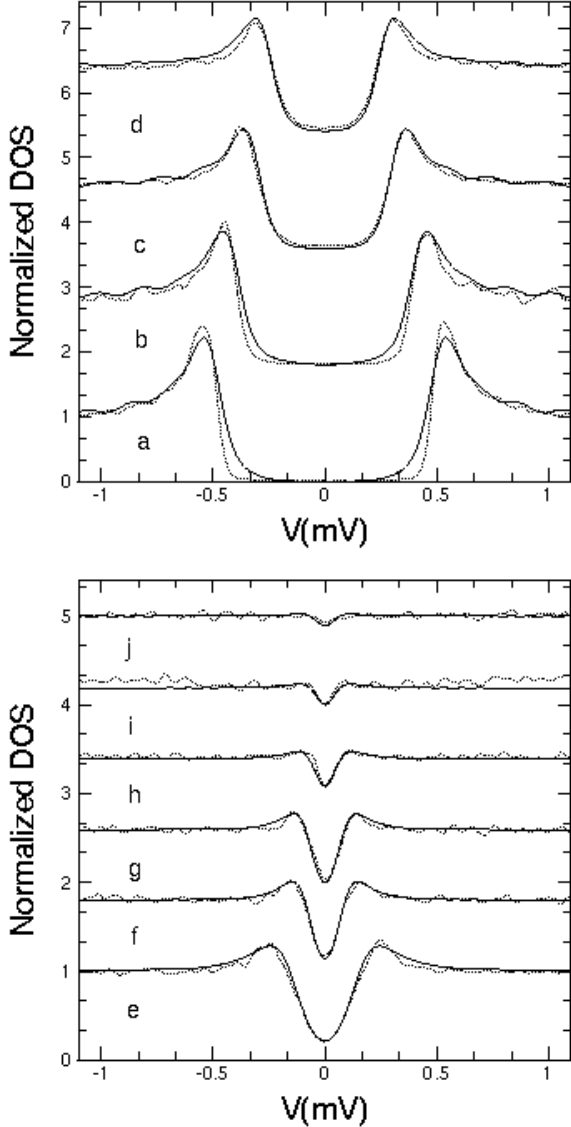


FIG. 25. Comparison of STM data from Ref. 37 with theory. Solid curves: theoretical results. Dotted curves: data. Vertical scales shifted for clarity. The labels *a* through *j* correspond to different probe positions. See text for details.

is unnecessary within the exact theory.

When the normal metal is a ferromagnet, experimental studies on the proximity effect are more sparse. The continuing advancement in nanofabrication techniques however, has made probing the electronic structure of *F/S* nanostructures experimentally accessible and some recent good quality data is available. We compare our theory with the tunnel spectroscopy data of Ref. 3 obtained through probing the local DOS in an Al superconductor adjacent to a Ni ferromagnet. Modifications to the DOS in the superconductor are another important aspect of the proximity effect which provides useful information regarding the influence of the ferromagnet on superconducting correlations. As predicted in Sec. III A 1

the local DOS near the interface in the superconductor should be substantially modified from the bulk BCS result. It is then of great interest to see how our results compare with the appropriate experiment.

To test our theory against the Al-Ni experimental data, we must choose a set of parameters appropriate for the given bilayer. Nickel itself is not a simple Stoner magnet with parabolic bands. A nearly free electron monovalent metal having the same saturation magnetization⁴⁶ as Ni, is easily seen to be to have a value of I of about 0.5 and this is the value we will use. We assume, a transparent interface ($H_B = 0$) in accordance with the clean interface in the experiment.³ We also take $T_c = 1.2$ K, $k_{FM} = 0.5 \text{ \AA}^{-1}$, and in order to limit as much as possible the number of input parameters, we keep the Fermi wave vectors the same, $\Lambda = 1$. For thick superconducting layers the relevant length which governs the depletion of superconducting correlations near the interface³⁴ scales with ξ_0 whenever $\xi_0 \gg 1$. In the experimental work, distances were already given in units of the correlation length, and this makes it particularly convenient to compare with theory. Experimental data is given at two distances: one far from the interface and the other near to it. The precise distance from the tunneling probe to the interface in the second case was somewhat uncertain, however, mainly because of the finite width of the probe. We take this position to be $2\xi_0$, which is similar to the value estimated in the experimental analysis.³

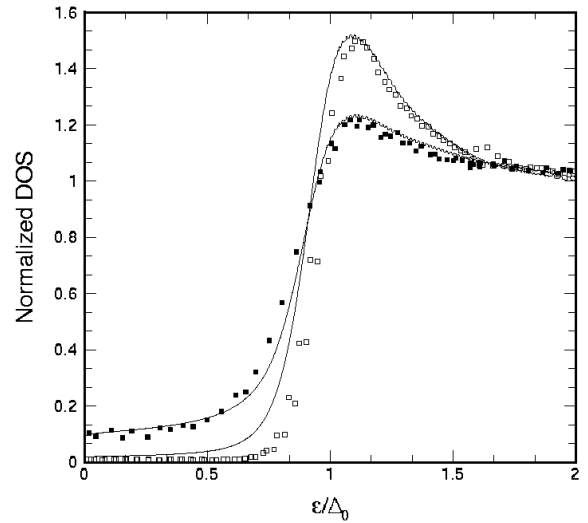


FIG. 26. Comparison of experimental DOS data for Ni-Al structure³ with theory. The symbols represent data taken far from the interface (open symbols) and near it (closed symbols). The curves are the theoretical fits obtained as explained in the text.

Figure 26 shows a fit of our results (solid lines) to the experimental data of Ref. 3. The vertical axis is the DOS scaled to the normal state value, while the energies are in dimensionless units of ϵ/Δ_0 . We account for the influence which single-charging effects have on the DOS by convolving the DOS calculated from (9) with the accep-

tance function $P(E)$ (as described in Ref. 3) that gives the probability for the junction to absorb an energy E .⁴⁸ The curve with the more prominent peak corresponds to the DOS in the bulk, away from the influence of the magnet, while the other curve is the DOS two coherence lengths from the interface. The open and closed symbols are the experimental results, the former ones being for the bulk DOS. The procedure employed to obtain these fits was the following: first we determined the effective temperature (to account for instrument resolution) by fitting our results to the experimental DOS near the interface, (closed symbols, solid curve). This resulted in a slightly raised effective temperature $T = 980$ mK (in contrast with the experimental value of $T = 100$ mK). Then, without any further changes, we calculated the DOS at a distance of $4\xi_0$ from the interface (dashed curve). This position should represent well the bulk characteristics in the DOS, since as we have seen previously, at that point, the influence of the ferromagnet on the superconducting DOS is minimal. No additional parameters were used to obtain this second fit. The results are clearly excellent: they have the correct peak positions and relative magnitudes. We therefore find again, good overall agreement with experiment in this more difficult case.

IV. CONCLUSIONS

We have in this work presented extensive results for the pair amplitude and local DOS in heterostructures involving superconductors and magnetic materials. These results were obtained from numerical, self-consistent solution of the Bogoliubov-deGennes equations, without approximations. We also discussed the length scales characterizing the influence of the superconductor on the ferromagnet and vice versa.

For heterostructures with geometric dimensions larger than the relevant intrinsic lengths, we have shown in detail how variation of parameters such as temperature T , Fermi wave vector mismatch Λ , interfacial and scattering strength H_B , (see Table I) affected the pair amplitude and local DOS for a wide range of exchange energies I . For $I = 0$, and low T , we find that the pair amplitude in the normal metal decays approximately as the inverse of the distance from the interface, with the overall prefactor depending on Λ and H_B . At higher temperatures, and for $\Lambda = 1$, $H_B = 0$, the decay markedly increases, and is set by a smaller length scale $\xi_N(T)$. The exact spatial decay of $F(\mathbf{r})$ was found to be more complicated than a single exponential. On the superconductor side, we tested our results for temperatures near T_c and found agreement with standard Ginzburg Landau theory. We also extracted the characteristic length of depletion $\xi_S(T)$ for intermediate and lower temperatures, something not previously done in a systematic way. The length scale (at low temperatures) characterizing the decline of $F(\mathbf{r})$ near the interface was found to decrease with smaller Λ

or larger H_B . The local DOS correlates with these results and displays a functional dependence on T , Λ , and H_B as well. We also systematically investigated the geometrical effects associated with the finite size of either the normal metal or superconductor and discovered that a small gap develops in the normal metal DOS when its width is small. This “mini-gap” decreases to zero when the metal width is close to the coherence length, i.e., $D_F \approx \Xi_0$.

At finite values of I , there are two characteristic proximity length scales ξ_2 and ξ_1 in the ferromagnet, governing respectively the spatial period of the damped oscillations in $F(\mathbf{r})$, and the sharp decay at the interface. Both lengths vary approximately inversely with I , independent of temperature. The amplitude of the damped oscillations however, decreases with increasing temperature. Mismatch of the Fermi energies increases the decay of the oscillations. A finite barrier strength has no effect on the period either, but does reduce the amplitude by a factor that scales linearly with H_B .

The damped oscillatory behavior in the ferromagnet induces a corresponding spatial modulation in the local DOS. For a transparent interface, the DOS in the superconductor side (for $I > 1/4$), exhibited a reduction in the usual BCS peaks, with a finite number of states within the gap, the number depending on the exchange field and location within the superconductor. For small exchange fields of order of $I \simeq \Delta_0/E_{FS}$, a significant subgap structure emerged and at exactly $I = \Delta_0/E_{FS}$, a resonance phenomenon occurred in which the BCS peaks became significantly enhanced. We found there exists a long range spin splitting in the superconductor, extending over several coherence lengths. A nontrivial behavior of δN was found as a function of I and the mismatch parameter Λ : when the point $E_{F\uparrow} = E_{FS}$ is crossed, the spin splitting becomes very short ranged, as found in Ref. 34.

Finally, we have compared our results with two sets of experimental data for the local DOS, corresponding to two different values of I and to measurements taken either from the superconductor or the non-superconductor side of the heterostructure. In both cases we found, using reasonable values for the material and geometric parameters, very good agreement between theory and experiment.

The number of relevant parameters involved is so large, and the variety of behaviors so rich, that even an extensive study such as this one must concentrate on the highlights and leave most of parameter space unexplored. It is clear however that the machinery developed here can be readily applied to most actual experimental situations. We hope that this paper will stimulate future experimental work and facilitate the analysis of the resulting data.

ACKNOWLEDGMENTS

We thank H. Courtois and M.A Sillanpää for providing us with their data.

[†] Electronic address: khalter@physics.umn.edu

^{*} Electronic address: otvalls@tc.umn.edu

- ¹ P.A. Kraus, A. Bhattacharya and A. M. Goldman, Phys. Rev. B **64**, 220505 (2001).
- ² A. N. Grogorenko *et al.* Phys. Rev. B **63**, 052504 (2001).
- ³ M.A. Sillanpää, T.T. Heikkila, R.K. Lindell, and P.J. Hakonen, Europhys Lett **56**, 590 (2001).
- ⁴ G. Deutscher and P.G. de Gennes, in *Superconductivity*, edited by R.D. Parks (Marcel Dekker, New York, 1969), p. 1005.
- ⁵ D.S. Falk, Phys. Rev. **132**, 1576 (1963).
- ⁶ P.G. de Gennes, *Superconductivity of Metals and Alloys* (Addison-Wesley, Reading, MA, 1989).
- ⁷ B.P. Stojković, and O.T. Valls, Phys. Rev. B **50**, 3374 (1994).
- ⁸ J. Hara, M. Ashida, and K. Nagai, Phys. Rev. B **47**, 11263 (1993).
- ⁹ E.A. Demler, G.B. Arnold, and M.R. Beasley, Phys. Rev. B **55**, 15 174 (1997).
- ¹⁰ Y. Blum, A. Tsukernik, M. Karpovskii, A. Palevski cond-mat/0203408.
- ¹¹ V. Prokic, A.I. Buzdin, and L.Dobrosavljevic-Grujic, Phys. Rev. B **59** 587 (1999).
- ¹² F.S. Bergeret, A.F. Volkov, and K.B. Efetov, cond-mat/0106510.
- ¹³ L.N. Bulaevskii, V. V. Kuzii JETP Lett. **25**, 290 (1977).
- ¹⁴ A.I. Buzdin, L.N. Bulaevskii, S.V. Panyukov, JETP Lett. **35**, 178 (1982).
- ¹⁵ A.I. Buzdin, B. Bujicic, M. Yu Kupriyanov, JETP Lett. **74**, 124 (1992).
- ¹⁶ P. Fulde and A. Ferrell, Phys. Rev. **135**, A550 (1964).
- ¹⁷ A. Larkin and Y. Ovchinnikov, Sov. Phys. JETP **20**, 762 (1965).
- ¹⁸ Z. Radovic, *et al.* Phys. Rev. B **44**, 759 (1991).
- ¹⁹ L.R. Tagirov, Physica C **307**, 145 (1998).
- ²⁰ Y.V. Fominov, N.M. Chitchev, and A.A. Golubov, cond-mat/0202280.
- ²¹ T. Kontos *et al.* cond-mat/0201104 (2002).
- ²² V.V. Ryazanov *et al.* Phys. Rev. Lett. **86**, 2427 (2001).
- ²³ M. Krawiec, B.L. Gyorffy, and J.F. Annett, cond-mat/0203184.
- ²⁴ Ya. V. Fominov and M.V. Feigelman, Phys. Rev. B **63**, 094518 (2001).
- ²⁵ I. Baladie and A. Buzdin, Phys. Rev. B **64** 224514.
- ²⁶ M. Zareyan, W. Belzig, and Yu. V. Nazarov, cond-mat/0107252.
- ²⁷ K.D. Usadel, Phys. Rev. Lett. **25**, 507 (1970).
- ²⁸ G. Eilenberger, Z. Phys. **214**, 195 (1968).
- ²⁹ Y. Tanaka and M. Tsukada, Phys. Rev. B **42**, 2066 (1990).
- ³⁰ I. Žutić and O.T. Valls, Phys. Rev. B **61**, 1555 (2000).
- ³¹ B.P. Vodopyanov, *et al.* Physica C, **366**, 31 (2001).
- ³² O. Bourgeois, *et al.*, Phys. Rev. B **63**, 064517 (2001).
- ³³ J. Aarts, *et al.*, Phys. Rev. B **56**, 2779 (1997).
- ³⁴ K. Halterman and O.T. Valls, Phys. Rev. B **65**, 014509 (2002).
- ³⁵ J-X. Zhu and C.S. Ting, Phys. Rev. B **61**, 1456, (2000).
- ³⁶ E. Vecino, A. Martin-Rodero and A. Levy Yeyati, Phys. Rev. B **64**, 184502 (2001).
- ³⁷ N. Moussy, H. Courtois, and B. Pannetier, Europhys. Lett. (2001).
- ³⁸ J.B. Ketterson and S.N. Song, *Superconductivity*, Cambridge University Press, (1999). See Ch. 41.
- ³⁹ S.W. Pierson and O.T. Valls, Phys. Rev. **B45**, 2458 (1992).
- ⁴⁰ P.G. de Gennes and D. St.-James, Phys. Lett. **4**, 151 (1963).
- ⁴¹ S. Pilgram, W. Belzig, and C. Bruder, Phys. Rev. B **62**, 12462 (2000).
- ⁴² K. Halterman, Ph.D. thesis, University of Minnesota, (2002).
- ⁴³ R. Fazio, and C. Lucheroni, Europhys. Lett. **45**, 707 (1999).
- ⁴⁴ G.E. Blonder, M. Tinkham, and T.M. Klapwijk, Phys. Rev. B **25**, 4415 (1982).
- ⁴⁵ B.P. Stojković, and O.T. Valls, Phys. Rev. B **47**, 5922 (1993).
- ⁴⁶ See Chapter 15 in C. Kittel *Introduction to Solid State Physics*, 7th edition, Wiley, New York (1996).
- ⁴⁷ S. Gueron, *et al.*, Phys. Rev. Lett. **77**, 3025 (1996).
- ⁴⁸ G.-L. Ingold and Yu. Nazarov, in *Single Charge Tunneling*, ed. by M.H. Devoret and H. Grabert, Plenum, N.Y. (1992).
- ⁴⁹ W. Belzig, C. Bruder, and G. Schon, Phys. Rev. B **54**, 9443 (1996).
- ⁵⁰ A.A. Golubov, Physica C, **326**, 46 (1999).